Immunity

Analysis of SARS-CoV-2 variant mutations reveals neutralization escape mechanisms and the ability to use ACE2 receptors from additional species

Graphical abstract

Highlights

- SARS-CoV-2 variants of concern are resistant to antibody neutralization
- B.1.351 variant is the most resistant, followed by P.1 and B.1.1.7
- The resistance hierarchy corresponds to mutations in NTD and RBD
- B.1.351 and P.1 acquire the ability to use mouse and mink ACE2 for entry

Authors

Ruoke Wang, Qi Zhang, Jiwan Ge, ..., Tong Zhang, Xinquan Wang, Linqi Zhang

Correspondence

zt_doc@ccmu.edu.cn (T.Z.), xinquanwang@mail.tsinghua.edu.cn (X.W.), zhanglinqi@tsinghua.edu.cn (L.Z.)

In brief

SARS-CoV-2 variants continue to emerge and spread around the world. Wang et al. conduct comprehensive mutational and crystal structure analyses of the variants and show that variants of concern, and the South African variant B.1.351 in particular, are resistant to many monoclonal antibodies and COVID-19 convalescent plasma and acquire the ability to use mouse and mink ACE2 receptors for infection.

Wang et al., 2021, Immunity *54*, 1611–1621
July 13, 2021
https://doi.org/10.1016/j.immuni.2021.06.003

Immunity

CellPress

Article

Analysis of SARS-CoV-2 variant mutations reveals neutralization escape mechanisms and the ability to use ACE2 receptors from additional species

Ruoke Wang,[1,2,12] Qi Zhang,[1,12] Jiwan Ge,[3,12] Wenlin Ren,[4,5] Rui Zhang,[1] Jun Lan,[3] Bin Ju,[6,7] Bin Su,[8] Fengting Yu,[9] Peng Chen,[1] Huiyu Liao,[8] Yingmei Feng,[8] Xuemei Li,[8] Xuanling Shi,[1] Zheng Zhang,[6,7] Fujie Zhang,[9] Qiang Ding,[4,5] Tong Zhang,[8,*] Xinquan Wang,[3,*] and Linqi Zhang[1,10,11,13,*]

[1]NexVac Research Center, Comprehensive AIDS Research Center, Center for Infectious Disease Research, Beijing Advanced Innovation Center for Structural Biology, School of Medicine, Tsinghua University, Beijing 100084, China

[2]Tsinghua-Peking Joint Center for Life Sciences, Beijing 100084, China

[3]The Ministry of Education Key Laboratory of Protein Science, Beijing Advanced Innovation Center for Structural Biology, Beijing Frontier Research Center for Biological Structure, Collaborative Innovation Center for Biotherapy, School of Life Sciences, Tsinghua University, Beijing 100084, China

[4]Center for Infectious Disease Research, School of Medicine, Tsinghua University, Beijing 100084, China

[5]Beijing Advanced Innovation Center for Structural Biology, Tsinghua University, Beijing 100084, China

[6]Institute for Hepatology, National Clinical Research Center for Infectious Disease, Shenzhen Third People's Hospital; The Second Affiliated Hospital, School of Medicine, Southern University of Science and Technology, Shenzhen 518112, Guangdong Province, China

[7]The Second Affiliated Hospital, School of Medicine, Southern University of Science and Technology, Shenzhen, China

[8]Beijing Youan Hospital, Capital Medical University, Beijing 100069, China

[9]Clinical and Research Center of Infectious Diseases, Beijing Ditan Hospital, Capital Medical University, No. 8, Jing Shun Dong Jie, Chaoyang, 100015 District Beijing, China

[10]Institute of Biopharmaceutical and Health Engineering, Tsinghua Shenzhen International Graduate School, Tsinghua University, Shenzhen 518055, China

[11]Institute of Biomedical Health Technology and Engineering, Shenzhen Bay Laboratory, Shenzhen 518132, China

[12]These authors contributed equally

[13]Lead contact

*Correspondence: zt_doc@ccmu.edu.cn (T.Z.), xinquanwang@mail.tsinghua.edu.cn (X.W.), zhanglinqi@tsinghua.edu.cn (L.Z.)

https://doi.org/10.1016/j.immuni.2021.06.003

SUMMARY

Severe acute respiratory syndrome coronavirus 2 (SARS-CoV-2) variants continue to emerge during the global pandemic and may facilitate escape from current antibody therapies and vaccine protection. Here we showed that the South African variant B.1.351 was the most resistant to current monoclonal antibodies and convalescent plasma from coronavirus disease 2019 (COVID-19)-infected individuals, followed by the Brazilian variant P.1 and the United Kingdom variant B.1.1.7. This resistance hierarchy corresponded with Y144del and 242–244del mutations in the N-terminal domain and K417N/T, E484K, and N501Y mutations in the receptor-binding domain (RBD) of SARS-CoV-2. Crystal structure analysis of the B.1.351 triple mutant (417N-484K-501Y) RBD complexed with the monoclonal antibody P2C-1F11 revealed the molecular basis for antibody neutralization and escape. B.1.351 and P.1 also acquired the ability to use mouse and mink ACE2 receptors for entry. Our results demonstrate major antigenic shifts and potential broadening of the host range for B.1.351 and P.1 variants, which poses serious challenges to current antibody therapies and vaccine protection.

INTRODUCTION

Current neutralizing antibody and vaccine strategies against severe acute respiratory syndrome coronavirus 2 (SARS-CoV-2), the causative agent of coronavirus disease 2019 (COVID-19), were developed by targeting the prototype SARS-CoV-2 strain identified during the early phase of the pandemic (Cao et al., 2020; Corbett et al., 2020; Hansen et al., 2020; Ju et al., 2020; Liu et al., 2020; Pinto et al., 2020; Robbiani et al., 2020; Vogel et al., 2021; Wang et al., 2020; Wu et al., 2020; Zhou et al., 2020; Zost et al., 2020). Several regulatory agencies recently approved a selection of these antibodies and vaccines for emergency use authorization (EUA), and their rollout to high-risk populations began late in 2020. Eli Lilly and Regeneron developed neutralizing monoclonal antibodies (mAbs) targeting the receptor-binding domain (RBD) of the spike (S) protein that have

been shown to reduce the viral loads of affected individuals, COVID-19-related symptoms, and hospitalizations (Chen et al., 2021; Gottlieb et al., 2021; Weinreich et al., 2021). We and others also reported the isolation and characterization several hundred RBD-specific mAbs from SARS-CoV-2-infected individuals (Cao et al., 2020; Hansen et al., 2020; Ju et al., 2020; Liu et al., 2020; Shi et al., 2020; Zost et al., 2020), some of which are under active clinical development. Pfizer/BioNtech and Moderna developed mRNA vaccines that express a stabilized form of the S protein, which demonstrated about 95% efficacy against symptomatic infection and a reduced risk of severe disease (Baden et al., 2021; Polack et al., 2020). Additional vaccine modalities, such as adenovirus-based, protein subunit, and inactivated vaccines, have also demonstrated reasonably good efficacy (Johnson & Johnson, 2021; Novavax, 2021; Voysey et al., 2021; Xia et al., 2021).

However, there is growing concern that the epidemic raging worldwide may be generating new SARS-CoV-2 variants that are antigenically distinct from the prototype strain, rendering current antibody and vaccine strategies ineffective (Callaway, 2021). By May 17, 2021 approximately 1,200,000 SARS-CoV-2 genome sequences were listed in the GISAID database, and more than 6,200 types of amino acid substitutions, deletions, and insertions have been found at least once in the S protein. Of the latter, 1,818 are in the N-terminal domain (NTD), 968 in the RBD, 741 in the subdomains 1 and 2 (SD1-2), and 2,481 in the S2 region (GISAID, 2021). Although these mutations are driven by the intrinsic, error-prone nature of the viral encoded RNA-dependent RNA polymerase (RdRp), their survival and maintenance rely on selective advantage during natural infection, transmission, and host adaptation. For example, the S protein D614G mutation became dominant just a few months into the pandemic and is associated with greater infectivity and transmissibility as well as moderately decreased susceptibility to antibody neutralization (Hou et al., 2020; Korber et al., 2020; Plante et al., 2021; Volz et al., 2021; Weissman et al., 2021; Yurkovetskiy et al., 2020). However, recently identified variants of SARS-CoV-2 (B.1.1.7 in the United Kingdom, B.1.351 in South Africa, and P.1 in Brazil) are raising serious concerns (England, 2020; Fujino et al., 2021; Kupferschmidt, 2021; Maggi et al., 2021; Tegally et al., 2021). They are not only rapidly displacing local SARS-CoV-2 strains but also carry NTD and RBD mutations that are critical for interactions with the ACE2 receptor and neutralizing antibodies (Barnes et al., 2020; Lan et al., 2020; Rambaut et al., 2020; Wang et al., 2021a; Yuan et al., 2020a). Specifically, B.1.1.7, B.1.351, and P.1 share the N501Y mutation, shown previously to enhance binding affinity to ACE2 (Laffeber et al., 2021; Tian et al., 2021). B.1.351 and P.1 each have three mutation sites in common within the RBD—K417N/T, E484K, and N501Y—which may change their antigenic profile. In addition, various deletion mutants are found in the NTD, such as 69–70del and Y144del in B.1.1.7 and 242–244del in B.1.351 (Rambaut et al., 2020; Tegally et al., 2021). A few mutations in the SD1-2 region near the Furin cleavage site are also identified, such as P681H in B.1.1.7 and A701V in B.1.351. Because all of these mutations fall in or are proximal to major S protein antigenic sites, they may adversely affect antibody neutralization induced by natural infection or vaccination.

To test the effect of these mutations on neutralization sensitivity, we generated a panel of 28 SARS-CoV-2 pseudoviruses corresponding to the identified mutations. These included 14 single mutations in the B.1.1.7, B.1.351, or P.1 variants, the K417N-E484K-N501Y mutation, and highly prevalent single mutations in the NTD, RBD, SD1-2, and S2 domains, identified across the entire S protein in the GISAID database (Figure 1A). The pseudoviruses were then subjected to neutralization tests against 12 human neutralizing mAbs, including some that had received EUA, some isolated initially from SARS-CoV-2-infected individuals in our laboratory, and 23 convalescent plasma samples collected from individuals with SARS-CoV-2 between January and February 2020. Our results show that B.1.351 was the most resistant to mAbs and convalescent plasma neutralization, followed by P.1 and then B.1.1.7. Such a resistance hierarchy was attributed to the extent of mutations identified in the NTD and RBD. Crystal structural analysis of the RBD carrying the triple K417N-E484K-N501Y mutation found in B.1.351 bound with the mAb P2C-1F11 revealed a molecular basis for antibody neutralization and escape. We also show that mutations acquired by B.1.351 and P.1 substantially improve their ability to use mouse and mink ACE2 for entry. These results demonstrate major antigenic shifts and the potential to broaden the host range of B.1.351 and P.1, posing serious challenges to current antibody therapies and vaccine protection.

RESULTS

SARS-CoV-2 variants show decreased susceptibility to mAb neutralization

We first evaluated the suspectability of the 28 pseudoviruses to neutralization by 12 mAbs, including 11 anti-RBD mAbs (4 mAbs approved with EUA and 7 other typical antibodies identified from SARS-CoV-2-infected individuals) and 1 epitope, well-defined anti-NTD mAbs 4A8. The anti-RBD mAbs fall into one of four major classes based on structural features affecting their mode of recognition and epitope specificity (Figure 1B; Barnes et al., 2020; Du et al., 2020; Ge et al., 2021; Hansen et al., 2020; Ju et al., 2020; Kreye et al., 2020; Pinto et al., 2020; Shi et al., 2020; Yuan et al., 2020a). These epitope assignments are related to the six major sites put forward by Yuan et al. (2021). The wild-type (WT) pseudovirus used throughout the analysis was the prototype strain with a D614G mutation (WT D614G). As shown in Figure 1C and Figure S1, the B.1.351 and P.1 pseudoviruses were more resistant to mAbs in terms of magnitude and breadth of neutralization relative to B.1.1.7. The B.1.351 and P.1 pseudoviruses were fully resistant to almost all class I and class II anti-RBD mAbs except for P2C-1F11, whereas class III and class IV were largely unaffected. Many mAbs had neutralizing activity below the detection limit (BDL) even when tested at the highest concentration (Figure 1C). The three variants were also resistant to the anti-NTD mAb 4A8, with the B.1.1.7 and B.1.351 pseudoviruses showing greater resistance relative to P.1.

Examination of the resistance patterns across the single- and triple-mutant pseudoviruses showed that the K417N and K417T mutations correlated with resistance to class I mAbs, whereas the E484K mutation correlated with resistance to class II mAbs

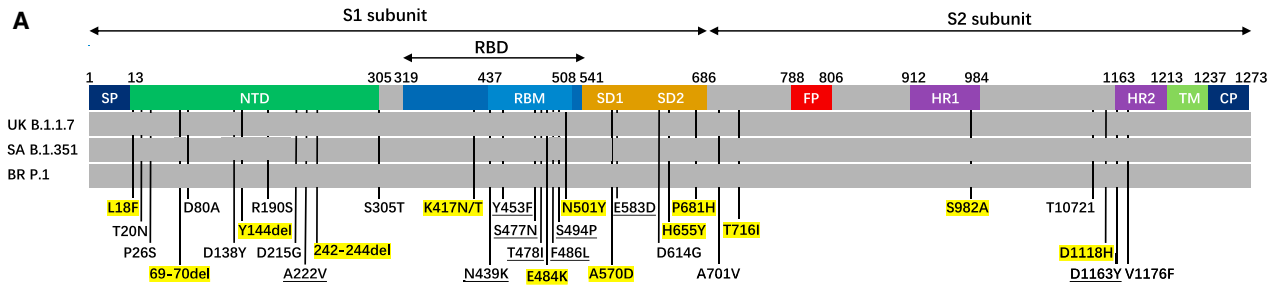

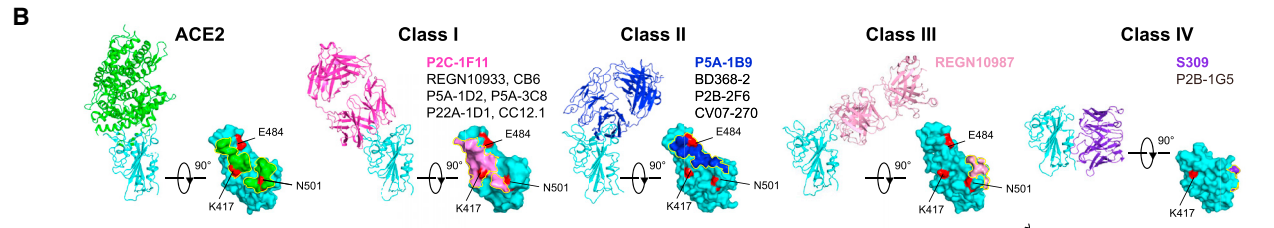

C

Fold changes in IC50		WT	Variants			NTD					RBD												SD1-2				S2			
		WT D614G	B.1.1.7	B.1.351	P.1	L18F	69-70del	Y144del	A222V	242-244del	K417N	K417T	N439K	Y453F	S477N	T478I	E484K	F486L	S494P	N501Y	417N/484K/501Y	A570D	E583D	H655Y	P681H	T716I	S982A	D1118H	D1163Y
anti-RBD	REGN10933	+1.0	+1.6	-13.0	-8.2	+1.2	-1.2	+1.2	-1.4	+1.0	-4.3	-7.0	-1.2	-47.3	+1.1	+1.7	-7.1	-35.0	-2.1	+1.5	-35.9	+1.7	+1.0	-1.2	+1.3	+1.5	+1.0	+1.3	+1.2
	CB6	+1.0	-4.9	BDL	BDL	+1.6	+1.5	+1.6	-1.7	+5.4	BDL	BDL	+2.6	+1.6	+2.0	+2.7	-2.4	-2.9	+1.7	-2.9	BDL	+4.7	+3.0	+1.9	+1.9	+2.5	+1.2	+1.9	+1.5
Class I	P2C-1F11	+1.0	+1.4	+2.2	+3.4	+1.0	+1.0	+1.2	-1.6	-1.0	-1.6	+1.5	-1.0	+1.0	+1.2	+1.6	-1.4	-3.1	+1.4	+1.0	+2.1	+1.9	+1.1	-1.1	-1.1	+1.8	-1.2	+1.0	-1.1
	P5A-1D2	+1.0	-3.3	BDL	BDL	-1.6	-1.0	-1.0	+1.1	-1.5	BDL	BDL	+1.1	-4.1	+1.0	-1.2	-1.6	-11.6	-1.5	-1.2	BDL	+1.7	-1.3	-1.3	-1.1	+2.2	-1.8	+1.5	+1.6
	P5A-3C8	+1.0	-2.2	BDL	BDL	+1.2	-1.1	+1.2	+1.1	+2.0	-24.9	BDL	+1.4	+1.3	+1.4	+1.5	+1.0	-1.0	+1.4	-1.8	BDL	+2.4	+1.7	+1.2	-1.0	+1.5	+1.3	+1.5	+1.5
	P22A-1D1	+1.0	-14.4	BDL	BDL	-1.2	+1.2	+1.5	+1.3	-1.6	BDL	BDL	-1.0	-5.0	+1.5	-1.1	-1.7	-2.3	+1.4	-7.1	BDL	+2.1	+1.0	-1.0	+1.2	+3.1	-1.0	+1.8	+2.1
Class II	BD368-2	+1.0	-1.3	BDL	BDL	-1.9	-2.1	-1.4	-2.1	-1.1	+1.1	-1.4	-2.3	-1.9	-1.2	-1.2	BDL	-1.4	-1.5	-1.2	BDL	-1.6	-1.5	-2.0	-1.6	+1.2	-1.1	-1.3	-1.0
	P5A-1B9	+1.0	-1.1	BDL	BDL	-1.8	-1.7	-1.4	-1.5	+1.5	+1.7	-1.1	-1.3	-1.3	-1.1	+1.1	BDL	BDL	+1.0	-1.2	BDL	+1.3	-1.3	-1.4	-1.4	-1.1	-1.1	-1.1	-1.1
Class III	REGN10987	+1.0	+2.4	+2.0	+3.0	-1.1	-1.3	-1.2	-1.3	+1.2	+1.4	-1.1	-26.6	+1.1	+1.3	+1.5	-1.3	+1.2	+1.2	+1.8	+1.5	+1.1	+1.0	-1.3	+1.2	+1.8	+1.3	+1.1	+1.0
Class IV	S309	+1.0	+2.1	+2.1	+1.4	-1.1	-1.1	-1.2	+1.2	+1.2	+2.6	+1.5	-1.0	-1.1	-1.0	+1.9	+1.4	+1.2	-1.5	+1.2	+1.2	-1.6	-1.8	-1.1	+1.2	+1.4	+1.0	+1.5	+1.9
	P2B-1G5	+1.0	+1.3	-6.0	+1.5	-1.9	-2.7	+1.2	-2.7	+1.0	+2.6	+1.3	+1.0	-1.5	-1.7	-1.5	-2.2	-2.1	-1.6	-2.6	-3.0	+1.2	-1.7	-3.6	-2.5	+1.1	-2.4	-1.9	-1.8
anti-NTD	4A8	+1.0	BDL	BDL	-7.9	+2.1	+1.4	BDL	+1.9	BDL	+4.2	+1.6	-1.0	+1.5	+1.8	+2.1	+1.0	+2.6	+1.1	+1.0	+1.8	-1.2	+1.2	-1.2	-1.1	+1.3	+1.4	+1.4	+1.4

D

Fold changes in surface binding		WT	Variants			NTD					RBD												SD1-2				S2			
		WT D614G	B.1.1.7	B.1.351	P.1	L18F	69-70del	Y144del	A222V	242-244del	K417N	K417T	N439K	Y453F	S477N	T478I	E484K	F486L	S494P	N501Y	417N/484K/501Y	A570D	E583D	H655Y	P681H	T716I	S982A	D1118H	D1163Y
anti-RBD	REGN10933	+1.0	+1.7	-5.8	-8.7	-1.6	-1.3	-2.6	+1.1	-1.9	+1.1	-1.0	-1.5	-50.9	-1.3	-1.6	-1.5	-2.6	-1.2	-1.3	-6.1	+1.0	-1.6	+1.2	-1.6	-2.0	+1.1	-1.3	-1.2
	CB6	+1.0	+1.8	-42.6	-18.7	-1.7	-1.2	-2.6	+1.2	-1.8	-21.9	-13.8	-1.6	-1.5	-1.3	-1.8	-2.0	-1.2	-1.2	-1.3	-28.5	+1.2	-1.8	+1.5	-1.4	-1.6	+1.4	-1.2	-1.5
Class I	P2C-1F11	+1.0	+2.5	+1.2	+2.6	-1.8	-1.2	-2.7	+1.1	-2.1	+1.7	+1.9	-1.8	-2.3	-1.5	-1.9	-2.4	-1.4	-1.6	-1.5	+1.2	+1.2	-2.1	+1.5	-1.6	-2.0	+1.5	-1.5	-1.4
	P5A-1D2	+1.0	+1.9	-19.8	-9.6	-1.5	-1.0	-2.8	+1.0	-2.8	-16.4	-12.9	-1.1	-1.5	-1.1	-1.2	-1.4	-2.0	-1.2	+1.1	-17.8	+1.9	-3.0	+2.0	+1.0	-1.5	+1.9	-1.1	-1.3
	P5A-3C8	+1.0	+3.3	-5.5	-2.9	-1.8	-1.1	-2.8	+1.4	-1.7	-1.3	-3.0	-1.8	-1.6	-1.3	-1.6	-1.9	-1.6	-1.4	+1.1	-4.4	+1.4	-1.9	+1.5	-1.4	-1.6	+1.8	-1.3	-1.2
	P22A-1D1	+1.0	+1.0	-35.7	-16.2	-2.3	-1.3	-3.8	-1.2	-2.1	-29.3	-27.4	-1.5	-1.6	-1.4	-1.6	-1.5	-1.3	-1.4	-1.8	-36.8	+1.3	-3.2	+1.7	-1.1	-1.3	+1.4	-1.1	-1.2
ClassII	BD368-2	+1.0	+1.4	-434.4	-192.1	-1.5	-1.2	-2.0	+1.3	-1.3	-1.0	+1.2	-1.5	-1.4	-1.3	-1.5	-569.4	-1.2	-1.3	-1.3	-221.5	-1.3	-1.4	+1.1	-1.3	-1.1	-1.1	-1.1	-1.1
	P5A-1B9	+1.0	+1.5	-48.2	-20.5	-1.5	-1.2	-2.0	+1.3	-1.3	-1.0	+1.2	-1.5	-1.6	-1.4	-1.6	-159.2	-17.8	-1.3	-1.3	-31.6	-1.2	-1.5	+1.1	-1.3	+1.0	+1.0	+1.0	-1.0
Class III	REGN10987	+1.0	+1.4	+1.1	+1.1	-1.5	-1.2	-2.0	+1.3	-1.3	-1.1	+1.2	-1.7	-1.5	-1.4	-1.5	-1.2	-1.3	-1.3	-1.3	-1.0	-1.3	-1.6	+1.1	-1.3	-1.1	-1.1	-1.1	-1.0
Class IV	S309	+1.0	+1.1	+1.9	-1.1	-1.7	-1.2	-2.0	+1.1	-1.1	+1.0	+1.1	-1.4	-1.7	-1.5	-1.6	+1.2	-1.3	-1.4	-1.2	+1.8	-1.5	-1.6	+1.2	-1.3	-1.7	-1.3	-1.2	+1.0
	P2B-1G5	+1.0	+2.6	-3.2	-1.5	-1.9	-1.2	-1.6	-1.0	-1.3	+1.4	+2.0	-1.0	-1.5	-1.2	-1.5	-3.2	-1.1	-1.1	-1.4	-2.1	+1.5	-1.9	+2.4	-1.3	-1.8	+2.4	+1.0	+1.0
anti-NTD	4A8	+1.0	-94.1	-109.0	-1.8	-1.0	+1.1	-909.2	+1.1	-718.0	-1.0	+1.2	-1.3	-1.4	-1.5	-1.5	-1.2	-1.3	-1.2	-1.1	+1.0	-1.1	-2.4	+1.2	-1.1	+1.2	+1.1	+1.1	-1.2
Soluble receptor	ACE2	+1.0	+22.1	+4.5	+5.2	-1.9	+1.4	-2.9	-1.0	-2.1	-6.4	-2.7	+1.6	+4.2	+2.8	-3.2	-1.0	-3.6	+1.4	+5.4	+4.3	+1.5	-1.7	+1.8	-1.2	-1.5	+1.4	+1.0	+1.1

Figure 1. SARS-CoV-2 variants and single amino acid mutations reduce neutralization and binding of mAbs

(A) Mutant residues along the S protein identified in SARS-CoV-2 variants B.1.1.7, B.1.351, and P.1. Mutant residues in each variant are indicated by black vertical lines. Those highlighted in yellow represent the mutant residues studied here. Nine mutant residues are underlined that were not identified in the three variants but included in the study because of their high representation in the GISAID database. SP, signal peptide; NTD, N-terminal domain; RBD, receptor-binding domain; RBM, receptor binding motif; SD, subdomain; FP, fusion peptide; HR1, heptad repeat 1; HR2, heptad repeat 2; TM, transmembrane domain; CP, cytoplasmic domain.

(B) The binding mode to and footprint of ACE2 and four classes of antibodies on the RBD. ACE2 is colored in green, RBD in cyan, and representative antibodies in four distinct colors. The three mutation residues (K417, E484, and N501) critical for binding to ACE2 and antibodies are shown in red.

(C and D) The fold changes in neutralizing activity, measured by half-maximal inhibitory concentration (IC_{50}) (C), and in binding activity, measured by mean fluorescence intensity (MFI), relative to that of WT D614G. "−" indicates increased resistance and "+" increased sensitivity. IC_{50} or MFI values highlighted in red indicate that resistance increased at least 3-fold; in blue, sensitivity increased at least threefold; and in white, resistance or sensitivity increased less than 3-fold. BDL (below the detection limit) indicates that the highest concentration of mAbs failed to reach 50% neutralization. Results were calculated from three independent experiments performed in technical duplicates.

See also Figures S1 and S2.

(Figure 1C). The triple-mutant K417N-E484K-N501Y pseudovirus, like B.1.351 and P.1, was resistant to class I and II mAbs, suggesting that combination of the three RBD mutations is key for conferring complete resistance. Neutralization by the 4A8 mAb was eliminated in two NTD deletion mutant pseudoviruses, Y144del and 242-244del. These deletions were initially identified in B.1.1.7 and B.1.351 and likely contribute to their resistance profiles (Chi et al., 2020; England, 2020; Tegally et al., 2021). Because both deletion mutations largely fall in the NTD supersite, B.1.1.7 and B.1.351 are likely resistant to other members of the same antibody family (Cerutti et al., 2021; Chi et al., 2020; Liu et al., 2020; McCallum et al., 2021; Suryadevara et al., 2021; Wang et al., 2021a).

Of note, the neutralization activities of mAbs approved for EUA (REGN10933, REGN10987, and CB6) or being studied for clinical use (P2C-1F11, BD368-2, S309, and P2B-1G5) were variably affected by pseudoviruses carrying these mutations (Figure 1C; Figure S1). The half-maximal inhibitory concentration (IC_{50}) of REGN10933 dropped 13.0- and 8.2-fold against B.1.351 and P.1, respectively, largely because of the K417N/T and E484K mutations (Figure 1C). Several mutations within the REGN10933 epitope, such as Y453F and F486L, were also

associated with a substantial reduction in neutralization. N439K, located in the REGN10987 epitope, showed a 26.6-fold reduction in IC_{50}. The most substantially affected mAb was CB6, one of the paired antibodies developed by Eli Lilly and approved for EUA, for which neutralization against B.1.351 and P.1 pseudoviruses was BDL when the highest concentration (1 μg/mL) was used. The reduction and loss of neutralization were largely attributed to K417N/T (Figure 1C). Despite being a class I or RBS-A antibody, P2C-1F11 was virtually unaffected by the mutations, as were the class III and IV anti-RBD mAbs REGN10987, S309, and P2B-1G5 (Figure 1C).

Next we studied the binding avidity of the 12 mAbs to the 28 mutant S proteins expressed on cell surfaces. There was a strong correlation between neutralization and binding avidity (Figure 1D; Figure S2), indicating that compromised binding avidity is a major escape mechanism. Last, soluble human ACE2 showed improved binding to all three variants as well as pseudoviruses bearing single N501Y and triple K417N-E484K-N501Y mutations (Figure 1D; Figure S2). This finding indicates that N501Y plays a role in enhanced binding, which is consistent with earlier reports of human and mouse ACE2 (Laffeber et al., 2021; Rathnasinghe et al., 2021; Sun et al., 2020; Tian et al., 2021). The single K417N mutation, however, decreased ACE2 binding by about 6.4-fold. These results indicate that the NTD mutations Y144del and 242-244del and the RBD mutations K417N/T, E484K, and N501Y confer substantial mAb resistance. The mAbs studied here with EUA would need to be optimized for the best possible efficacy against new variants.

Structural basis for mAb neutralization and escape

We next studied the structural basis for the mAb P2C-1F11 which is able to maintain neutralization to the variants despite being a class I or RBS-A anti-RBD antibody. We determined the crystal structure of the SARS-CoV-2 RBD carrying K417N-E484K-N501Y mutations (RBD-3M) bound by P2C-1F11 at a resolution of 2.10 Å (PDB: 7E8M; Table S1). Comparing this structure with our previously reported crystal structure of the WT RBD with P2C-1F11 at 3.0 Å (PDB:7CDI), we found that the three mutations did not change the overall binding mode of P2C-1F11 to the RBD (Figure 2A), as evidenced by a 0.52 Å root-mean-square deviation (RMSD) value for all 581 Cα atoms. However, a couple of subtle changes were identified. One was related to the interactive forces with residue 417 and the other with residue 501. Like other class I and RBS-A antibodies, P2C-1F11 bound to WT K417 through hydrophobic and hydrogen bond interactions. This was largely mediated by its heavy-chain germline residues Y33 and Y52 (Ge et al., 2021). These interactions were diminished by the K417N mutation but replaced by one hydrogen bond between Y52 and mutant N417 (Figure 2B; Table S2). Furthermore, unlike those in class I or RBS-A, P2C-1F11 did not form salt bridge interactions between aspartic acid (D) and K417 (Figures 2B and 2C). The K417N mutation would therefore be less disruptive to P2C-1F11 than to those in class I or RBS-A, such as P5A-1D2, P22A-1D1, and CB6, studied here, and CC12.1, CC12.3, COVA2-04, and COVA2-07, characterized elsewhere (Ge et al., 2021; Yuan et al., 2020a).

Structural analysis showed that the P2C-1F11 light chain had extensive interactions with RBD-3M residues Y453, Q493, T500, and Y501 around the 501 position but much less interaction with the WT RBD residue asparagine (N) at the 501 position (Figure 2B; Table S2). The extra interactions between RBD-3M and P2C-1F11 around Y501 may also contribute to the retained binding and neutralization of P2C-1F11 against SARS-CoV-2 variants carrying the triple K417N-E484K-N501Y mutation.

Similar to the WT RBD, P2C-1F11 did not directly bind to E484K in RBD-3M (Figure 2B; Table S2). This explains why E484K had no detectable effect on the binding and neutralizing activity of P2C-1F11. However, the E484K mutation resulted in complete loss of BD368-2 and P5A-1B9 neutralization (Figure 1C; Figure S1). Structural analysis showed that the E484 formed salt-bridge and/or hydrogen-bonding interactions with BD368-2, P5A-1B9, P2B-2F6, and CV07-270 (Figure 2D; Du et al., 2020; Ju et al., 2020; Kreye et al., 2020). Therefore, the E484K mutation would diminish such interaction and render this class of antibodies ineffective against B.1.351 and P.1.

Next we measured the equilibrium dissociation constants and calculated K_D values of P2C-1F11 binding to the WT RBD and RBD-3M. Consistent with the neutralization results, binding of P2C-1F11 in Fab or full-length immunoglobulin G (IgG) form to RBD-3M was slightly weaker compared with the WT RBD (21.9 versus 14.4 nM and 8.9 versus 2.2 nM, respectively; Figure S3). Furthermore, antibodies that lost their neutralizing activities, including CB6, P5A-1D2, P5A-3C8, P22A-1D1, BD368-2, and P5A-1B9, failed to show detectable levels of binding to RBD-3M (Figure S3). These results indicate that antibody binding activity correlates well with antibody neutralizing activities.

SARS-CoV-2 variants reduced sensitivity to neutralization by convalescent plasma

We next studied the degree to which major variant pseudoviruses conferred resistance to convalescent plasma from SARS-CoV-2-infected individuals. Plasma samples were collected from 23 affected individuals during the early wave of the pandemic between January and February of 2020. Fourteen of these individuals had only mild symptoms, and nine developed severe disease. The average age was 56 with a range of 29–81 years of age. Thirteen were men, and ten were women (Table S3). For each plasma sample, eight serial dilutions were made, starting from 1:60 or 1:200, and neutralization activity was estimated based on half-maximal inhibitory dilution (ID50) and fold changes relative to that against the WT D614G pseudovirus (Figure 3; Figure S4). Overall, neutralizing activity was higher in serum from those with severe versus those with mild disease (Figures 3A and 3B). Consistent with the findings for mAbs, the B.1.351 and P.1 pseudoviruses demonstrated more resistance than B.1.1.7 in absolute ID50 (Figures 3A and 3B) and fold changes (Figure 3C) relative to WT D614G. The average reductions in neutralization activity across the 23 plasma samples were at least 6.9-fold against the B.1.351, 2.4-fold against the P.1, and no significant reduction against the B.1.1.7 pseudovirus (Figure 3A). Complete loss of neutralization activity, indicated by BDL in Figure 3C, was observed for 11 plasma samples against pseudovirus B.1.351, four against P.1, and none against B.1.1.7. The remaining plasma demonstrated varying degrees of reduction in neutralization potency.

Examination of the resistance patterns across the single- and triple-mutant pseudoviruses revealed some notable patterns. In

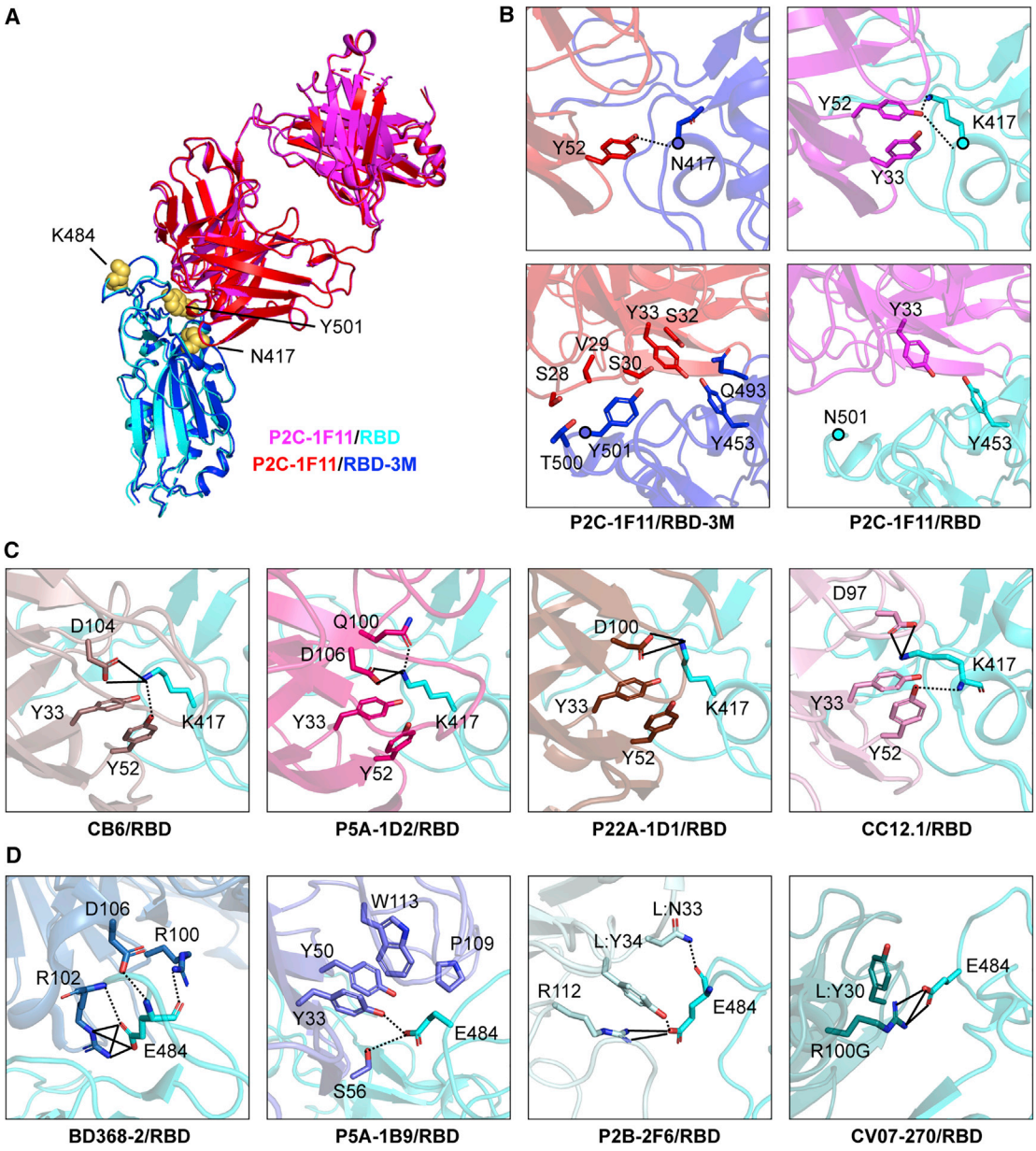

Figure 2. Structural basis for mAb neutralization and escape

(A) P2C-1F11/RBD-3M crystal structure superimposed onto the P2C-1F11/RBD crystal structure (PDB: 7CDI). P2C-1F11 is colored magenta and RBD is colored cyan in the P2C-1F11/RBD complex. P2C-1F11 and RBD-3M are colored red and blue, respectively, in the P2C-1F11/RBD-3M complex. The three RBD-3M mutated residues (N417, K484, and Y501) are shown as yellow spheres.

(B) Interactions with P2C-1F11 around RBD-3M N417 and Y501 (left panel) and WT RBD K417 and N501 (right panel).

(C) Interactions between K417 and the representative class I IGHV3-53/3-66 antibodies CB6, P5A-1D2, P22A-1D1, and CC12.1.

(D) Interactions between E484 and the class II antibodies BD368-2, P5A-1B9, P2B-2F6, and CV07-270.

In (C) and (D), antibodies are shown with different colors; hydrogen bond and salt bridges are represented by dashed and black lines, respectively. CB6/RBD (PDB: 7C01), P5A-1D2/RBD (PDB: 7CHO), P22A-1D1/RBD (PDB: 7CHS), CC12.1/RBD (PDB: 6XC2), BD368-2/RBD (PDB: 7CHC), P5A-1B9 (PDB: 7CZX), P2B-2F6 (PDB: 7BWJ), CV07-270 (PDB:6XKP). See also Figure S3 and Tables S1 and S2.

particular, the 242–244del mutation in the NTD reduced neutralization activity more than 2-fold for 5 of 23 samples (C-Plasma1, C-Plasma5, C-Plasma7, C-Plasma8, and C-Plasma9), which correlated with the reduction or loss in potency observed against B.1.351 pseudoviruses (Figure 3C; Figure S4). The NTD supersite antibodies were likely to account for such a significant reduction (Cerutti et al., 2021; Chi et al., 2020; McCallum et al., 2021). On the other hand, the single-mutant E484K and triple-mutant K417N-E484K-N501Y pseudoviruses substantially reduced the neutralization activity for 8 of 23 samples (C-Plasma6, C-Plasma10, C-Plasma15, C-Plasma16, C-Plasma17, C-PlasmaP#2, C-PlasmaP#5, and C-PlasmaP#22), which

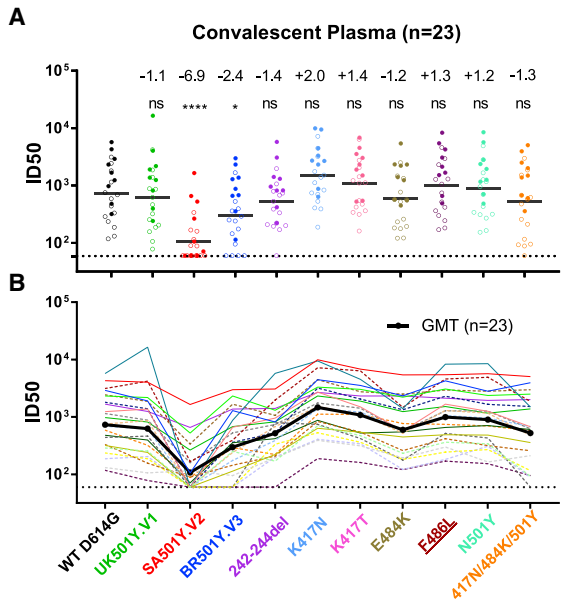

C

Fold changes in ID50	WT	Variants			NTD	RBD					
C-Plasma1	+1.0	-1.5	-27.6	-2.3	-3.6	+1.5	+1.2	-1.2	+1.5	-1.0	+1.4
C-Plasma2	+1.0	-1.1	-2.6	-1.4	-1.4	+2.3	+1.6	+1.3	+1.3	+1.3	+1.2
C-Plasma3	+1.0	-1.2	-3.7	-1.4	-1.2	+2.4	+1.9	+1.3	+1.6	+1.2	+1.4
C-Plasma4	+1.0	-1.3	-2.5	-1.2	-1.2	+1.6	+1.4	+1.4	+1.3	+1.2	+1.2
C-Plasma5	+1.0	-1.8	-6.7	-2.0	-2.7	+1.9	+1.9	+1.3	+1.3	+1.2	-1.0
C-Plasma6	+1.0	-1.3	-7.2	-2.2	-1.6	+1.5	+1.2	-2.0	+1.1	+1.1	-1.9
C-Plasma7	+1.0	-1.3	-7.2	-1.5	-2.3	+1.8	+1.1	+1.0	+1.2	+1.2	+1.2
C-Plasma8	+1.0	-1.3	BDL	-5.0	-3.4	+1.8	+1.1	-1.3	+1.3	-1.1	-1.2
C-Plasma9	+1.0	-1.5	BDL	BDL	BDL	+1.6	+1.4	+1.0	+1.4	+1.3	-1.2
C-Plasma10	+1.0	+1.3	-18.7	-8.0	-1.6	+2.3	+2.0	-2.1	+1.5	+1.6	-1.7
C-Plasma11	+1.0	-1.2	-6.7	-1.4	-1.1	+1.8	+1.1	+1.1	+1.4	+1.5	+1.3
C-Plasma12	+1.0	+1.1	BDL	-3.1	-1.1	+2.0	+1.5	-1.4	+1.7	+1.5	-1.6
C-Plasma13	+1.0	-1.1	-4.4	-1.0	-1.8	+1.4	+1.3	-1.0	+1.3	+1.0	+1.1
C-Plasma14	+1.0	-1.1	BDL	-3.9	-1.8	+2.0	+1.8	-1.2	+1.5	+1.4	-1.0
C-Plasma15	+1.0	+1.1	BDL	BDL	+1.1	+2.2	+1.8	-1.5	-1.0	+1.7	-2.1
C-Plasma16	+1.0	+1.1	BDL	BDL	+1.8	+1.7	-1.0	-2.5	+1.2	-1.0	BDL
C-Plasma17	+1.0	-1.3	BDL	BDL	+1.4	+2.3	+1.5	-1.3	+1.0	+1.1	-2.0
C-Plasma18	+1.0	-2.1	-3.7	-2.3	-1.6	+2.5	+1.6	-1.3	+1.3	-1.0	-1.3
C-Plasma19	+1.0	-1.2	-1.1	-1.4	+1.5	+3.0	+2.4	+1.5	+2.3	+1.3	+1.6
C-Plasma20	+1.0	-1.3	BDL	-2.8	-1.4	+2.0	+1.7	+1.4	+1.5	+1.5	+1.1
C-Plasma P#2	+1.0	+2.9	BDL	-6.5	+1.0	+1.6	-1.3	-4.1	+1.4	+1.5	-3.8
C-Plasma P#5	+1.0	+1.1	BDL	-1.9	-1.3	+2.2	+1.2	-2.2	+1.4	+1.0	-1.8
C-Plasma P#22	+1.0	-1.1	BDL	-1.1	-1.7	+2.4	+1.6	-1.2	+1.3	+1.2	-3.1
C-Plasma Standard	+1.0	BDL	BDL	+4.3	BDL	+1.5	+1.1	+1.3	+2.0	+1.1	+1.0

WT D614G, B.1.1.7, B.1.351, P.1, 242-244del, K417N, K417T, E484K, F486L, N501Y, 417N/484K/501Y

Figure 3. SARS-CoV-2 variants reduced sensitivity to convalescent plasma neutralization

Reciprocal plasma dilutions (ID50) against SARS-CoV-2 variants are shown by (A) colored dots or (B) colored curves, each of which represents a different convalescent plasma. The geometric mean against each variant is indicated by a black horizontal line in (A) and black curve (B). Plasma samples from individuals with mild and severe disease are indicated by empty or solid circles in (A) and dashed or solid curves in (B). The fold change in ID50 between mutant and WT D614G pseudoviruses is shown by overall average at the top in (A) or individually in (C). "−" indicates an increase in resistance, and "+" indicates an increase in sensitivity. In (C), red highlights indicate a minimum 2-fold increase in resistance; blue a minimum 2-fold increase in sensitivity, and white a less than 2-fold change in resistance or sensitivity. BDL indicates that the highest concentration of plasma (1:60) failed to confer 50% neutralization. Standard plasma was obtained from the NIBSC (code: 20/136). Results of 23 plasma samples and standard plasma were calculated from three independent experiments performed in technical duplicates. *$p < 0.05$; and ****$p < 0.0001$; ns, not significant. See also Figure S4.

corresponded to their diminished or loss of neutralization against the B.1.351 and P.1 pseudoviruses. Antibodies targeting the receptor binding motif (RBM) likely contributed to such changes (Figure 3C; Figure S4). In contrast, for pseudoviruses carrying only the K417N mutant, neutralization efficacy invariably increased for all plasma sample studied, with an average 2.0-fold improvement. A similar trend was also seen for pseudoviruses carrying only the K417T mutant (Figure 3C; Figure S4). The single mutant N501Y pseudovirus, reported previously to enhance ACE2 binding (Laffeber et al., 2021; Chan et al., 2021; Tian et al., 2021), had limited effects on the neutralizing activity of convalescent plasma.

Last, the plasma standard (code 20/136) obtained from the NIBSC (United Kingdom) failed to neutralize the B.1.1.7 and B.1.351 pseudoviruses, which correlated with loss of efficacy against the 242–244del pseudovirus (Figure 3C; Figure S4). This suggests that anti-NTD antibodies account for a major proportion of neutralizing activity in this sample. These results indicate that B.1.351 was the most resistant pseudovirus against the convalescent plasma tested, followed by P.1 and then B.1.1.7. The loss of plasma neutralizing activities is attributed, to varying degrees, to the 242–244del in the NTD, E484K, and triple K417N-E484K-N501Y mutations in the RBD, depending on individual plasma. Different convalescent plasma appears to respond differently to the mutated pseudoviruses, perhaps reflecting the different compositions and proportions of neutralizing antibodies in each individual generated during natural infection.

Enhanced entry of SARS-CoV-2 variants through mouse and mink ACE2

To study the potential effect of SARS-CoV-2 variants on host range and cross-species transmission, we characterized the ability of ACE2 from nine host species to support entry of 28 SARS-CoV-2 mutant pseudoviruses. HeLa cell lines stably expressing the ACE2 molecules were subjected to infection. The entry efficiency was measured and presented as fold change relative to WT D614G. As shown in Figure 4, the three variants B.1.1.7, B.1.351, and P.1 gained substantial ability to infect HeLa mouse ACE2, which correlated with pseudoviruses bearing single (K417N, K417T, E484K, and N501Y) and triple (K417N-E484K-N501Y) mutations. This agreed well with recent reports where single N501Y or triple K417N-Q493H-N501Y mutations were found in the mouse-adapted SARS-CoV-2 strains, although the triple mutant causes more severe acute respiratory symptoms and mortality in standard laboratory mice (Rathnasinghe et al., 2021; Sun et al., 2020). Single N501Y mutations found in B.1.1.7 and two of three (K417N and N501Y) found in B.1.351 and P.1 therefore likely enhanced binding to mouse ACE2, improving entry efficiency into HeLa mouse ACE2.

The single-mutant E484K pseudovirus also enhanced entry into HeLa mouse ACE2 and HeLa mink ACE2. Such enhancement occurred only with the E484K-bearing variant B.1.351 and P.1 but not with the E484K-missing variant B.1.1.7, suggesting that the added and/or synergistic effect of E484K with other mutant residues facilitates entry into these two cell lines. Furthermore, two single-mutant pseudoviruses, Y453F and F486L, also

Fold changes in entry	WT	Variants			NTD					RBD												SD1-2				S2			
	WT D614G	B.1.1.7	B.1.351	P.1	L18F	69-70del	Y144del	A222V	242-244del	K417N	K417T	N439K	Y453F	S477N	T478I	E484K	E486L	S494P	N501Y	417N/484K/501Y	A570D	E583D	H655Y	P681H	T716I	S982A	D1118H	D1163Y
HeLa Human-ACE2	+1.0	-6.6	-1.0	-1.9	+1.5	+1.9	-1.6	-2.4	-3.4	-1.3	+1.2	-3.6	-2.0	-1.4	-3.2	-2.3	-1.5	-1.8	-3.6	-1.8	-2.0	-3.6	-1.3	-1.7	-10.6	-2.5	-1.1	-2.4
HeLa Erbat-ACE2	+1.0	-3.8	+1.3	-1.3	+2.4	+2.6	-1.0	-1.4	-5.8	-97.1	-38.4	-1.9	-4.0	-1.0	-3.1	-1.7	+2.0	-1.3	-1.4	-1.7	+1.1	-3.5	+1.6	-1.6	-16.5	-3.8	-1.2	-2.3
HeLa Rsbat-ACE2	+1.0	-5.5	-37.8	-79.4	+1.6	+1.8	-2.0	-1.9	-6.7	-2.1	-1.5	-3.4	-2.5	-1.3	-2.9	-8.8	-1.7	-1.5	-3.6	-195.8	-1.8	-3.3	+1.1	-1.7	-11.4	-2.4	-1.1	-2.7
HeLa Pangolin-ACE2	+1.0	-6.5	-1.2	-1.5	+1.8	+2.4	-2.0	-2.0	-2.6	-1.0	+1.3	-3.0	-1.8	-1.2	-2.3	-2.2	-1.1	-1.3	-2.6	-2.0	-1.9	-3.1	+1.3	-1.8	-9.8	-1.7	+1.1	-2.2
HeLa Pig-ACE2	+1.0	-8.2	-1.3	-2.6	+1.3	+1.7	-2.2	-2.3	-3.0	-1.2	+1.0	-3.5	-2.2	-1.5	-2.7	-2.4	-1.1	-1.8	-3.4	-2.3	-2.1	-3.7	-1.2	-1.9	-12.1	-2.2	-1.1	-2.4
HeLa Cat-ACE2	+1.0	-5.3	-1.1	-2.3	+1.0	+1.1	-3.7	-2.5	-1.9	+1.1	+1.1	-4.0	-2.7	-1.7	-3.1	-1.5	-1.5	-1.5	-3.3	-1.9	-2.5	-2.6	-1.2	-2.2	-11.0	-2.0	-1.1	-1.8
HeLa Dog-ACE2	+1.0	-6.1	-1.2	-2.4	+1.1	+1.1	-3.9	-2.9	-1.9	+1.1	+1.0	-4.7	-2.9	-2.0	-3.6	-1.6	-1.7	-1.6	-3.8	-2.8	-2.9	-2.6	-1.3	-2.3	-10.0	-1.8	-1.1	-1.9
HeLa Mink-ACE2	+1.0	-1.2	+10.0	+4.3	-1.3	+2.9	-11.3	-1.4	-4.9	-2.8	-14.5	+2.3	+21.9	+1.0	-3.8	+26.6	+31.7	+4.0	+3.5	+3.0	+1.8	-4.3	+1.7	-2.3	-11.3	-5.2	+1.1	-2.3
HeLa Mouse-ACE2	+1.0	+26.6	+108.0	+71.7	+1.6	+3.8	+1.5	-1.4	-12.7	+23.1	+32.0	-9.7	-3.5	-1.3	-2.4	+24.0	+2.6	+3.0	+41.5	+44.7	+2.1	-4.7	+1.2	-1.3	-17.3	-5.8	-1.0	-3.5

Figure 4. Entry efficiency of SARS-CoV-2 variants into HeLa cells expressing ACE2 from diverse host species

The values show the fold changes in luciferase activity for each indicated mutant pseudovirus variant compared with WT D614G. "+" indicates an increase in entry efficiency, and "−" indicates a decrease. Red highlights indicate at least a 3-fold increase in efficiency; blue indicates at least a 3-fold decrease in efficiency, and white indicates no change greater than 3-fold. Results were calculated from three independent experiments performed in technical triplicates.

substantially improved entry efficiency. These two mutations have been found recently among the mink-associated SARS-CoV-2 circulating in mink farms in Denmark, suggesting their critical role in adaptation and transmission among the mink population (Oude Munnink et al., 2021). In contrast, entry efficiency through ACE2 of the other animal origins was reduced substantially, particularly for B.1.1.7 (Figure 4). For B.1.351 and P1, entry remained largely unchanged, except for Rsbat-ACE2 (Figure 4). These results indicate that the three variants, particularly B.1.351 and P.1, acquired mutations in the RBD that not only facilitated their escape from antibody neutralization but also potentially expanded their host range to mice and mink. Active surveillance of these variants in humans and relevant animal species would be required to minimize potential cross-species transmission.

DISCUSSION

In this study, we evaluated the effect of mutations found in the emerging SARS-CoV-2 variants B.1.1.7, B.1.351, and P.1, as well as some single mutations within or close by the major antigenic sites in the S protein identified in the GISAID database. We identified K417N, E484K, and N501Y mutations in the RBD of the three variants that have profound consequences on antibody neutralization and interaction with mouse and mink ACE2. Mutations in the NTD also substantially reduced neutralizing sensitivity to supersite antibodies as well as convalescent plasma, suggesting that NTD and RBD responses may be contributing jointly to overall protection in polyclonal responses. Because responses to the NTD or RBD can be readily diminished by escape mutations, targeting both regions may be more advantageous. Our entry studies were conducted on ectopically expressed mouse and mink ACE2 and are not necessarily equivalent to natural infection and transmission in the corresponding animals. However, the same K417N and/or N501Y mutations found in mouse-adapted SARS-CoV-2 should raise enough concern about the potential spread of these new variants to mice and beyond. Indeed, recently identified SARS-CoV-2 variants in a mink farm in Denmark have raised another warning sign regarding the complexity of host range and cross-species transmission of SARS-CoV-2 variants. Rigorous and thorough monitoring of relevant animals would be required to better understand such complexity and prevent future outbreaks.

Among the three variants, B.1.351 was the most resistant against mAbs and convalescent plasma, followed by P.1 and then B.1.1.7. This resistance hierarchy corresponded well to genetic mutations in the NTD and RBD that led to major antigenic changes in the S protein. Particularly B.1.351 had the NTD supersite mutation (242–244del) and triple K417N-E484K-N501Y RBD mutation, whereas P.1 had only the latter and B.1.1.7 only the former (Y144del) together with N501Y in the RBD (Figure 1A). The effect of these mutations on conferring antibody resistance clearly indicates that NTD and RBD are major antigenic domains on the S protein. Of note, 5 of 23 plasma samples had a more than 2-fold loss-neutralizing ability resulting from 242–244del alone, and another 5 of 23 plasma samples had a more than 2-fold loss of neutralizing ability resulting from 484K alone, indicating that some people reacted in a more focused way to one epitope and, thus, may be more vulnerable to common circulating variants. Further study is needed to precisely estimate the relative contributions of RBD-directed and NTD-directed neutralizing antibodies to overall plasma neutralizing activity. To date, the most potent mAbs isolated from infected and vaccinated individuals are often dominated by those targeting the RBD, whereas many isolated NTD mAbs failed to reach 100% potency in neutralizing activity (Chi et al., 2020; Hansen et al., 2020; Ju et al., 2020; Liu et al., 2020; Robbiani et al., 2020; Wang et al., 2021b; Zost et al., 2020; McCallum et al., 2021). These results point to a greater effect of RBD antibodies in overall plasma neutralization. Nevertheless, new SARS-CoV-2 variants with increasing numbers of mutations in the NTD and RBD will challenge the efficacy of mAb therapies and vaccine protections.

The effects of these mutations, in terms of mAbs, are clear. B.1.351 and P.1 are resistant to neutralization by many anti-RBD and anti-NTD antibodies, including two (CB6 and REGN10933) already approved for EUA (FDA, 2021; Wang et al., 2021a; Huang et al., 2021; Wang et al., 2021b). Most class I mAbs studied here were disrupted by the K417N/T mutation and those in class II by the E484K mutation. Of note, we observed that the single K417N/T mutant tended to increase rather than decrease the neutralizing activity of non-class I mAbs. Because K417N/T also markedly reduced binding to soluble ACE2, this mutation may shift the balance in favor of binding to an antibody rather than to ACE2. Similar findings were also found for convalescent plasma. More importantly, P2C-1F11, which is currently in therapeutic development, was virtually unaffected by the single K417N/T or the triple K417N-E484K-N501Y mutation. The ability of Y52 in its heavy chain to maintain a

hydrogen bond with the mutant N417 while gathering more interactive forces around mutant Y501 provides plausible structural explanations (Figure 2; Table S2). This was verified by similar binding activity of P2C-1F11 to the WT RBD and RBD-3M, indicating that antibody binding activity was well correlated with their neutralizing activities. Considering that most class I antibodies with heavy-chain IGHV3-53/3-66 usage lost efficacy against the K417N mutation, the P2C-1F11 findings show the existence of class I antibodies that were not affected by the mutation. This offers hope for inducing P2C-1F11-like antibodies by vaccine that can maintain strong, broadly neutralizing activity against a wide range of variants, including B.1.351 and P.1.

For convalescent plasma, the most profound effect was observed on the B.1.351 pseudovirus, followed by P.1 and then B.1.1.7. Reduction or complete loss of neutralization activities were variably attributed to the 242–244del mutation in the NTD, E484K, and triple K417N-E484K-N501Y in the RBD, depending on the individual profiles of neutralizing antibodies. Similar reductions in neutralization of B.1.351 have also been reported elsewhere for recovered individuals and individuals vaccinated with mRNA or inactivated vaccines approved under EUA (FDA, 2021; Wang et al., 2021a; Huang et al., 2021; Wang et al., 2021b). Although the specific levels of neutralizing antibody required to confer protection remain uncertain, reductions in antibody titers raise concerns regarding their protective potential against emerging variants, particularly B.1.351. Indeed, reductions in antibody titers have been associated with an increased likelihood of re-infection (Sabino et al., 2021). Recent vaccine trials in South Africa showed reduced efficacy against B.1.351 but maintained efficacy against WT strains (Diamond et al., 2021; Hoffmann et al., 2021; Wu et al., 2021). These results demonstrate that antigenic shifts are occurring among emerging SARS-CoV-2 variants. This calls for immediate reevaluation and updates of mAb therapies and vaccines. In the long run, the goal is to develop universal therapeutic and preventive interventions that maintain efficacy against all strain mutations. Until then, control over the emergence of new variants requires accelerated vaccine rollouts and ardent practice of proven public health measures.

LIMITATIONS OF STUDY

We note some limitations associated with our study. First, the ACE2 usage data relied on ectopically expressed ACE2 on the surface of human HeLa cells that may not reflect the levels and conformations on their original native cells. Reverse zoonotic infection would need to be verified through future relevant animal studies. Second, because of the limited amount of serum samples, we used 1:60 as our first dilution in the neutralization assay, which may underestimate the effect of variants on neutralization escape. Third, we were only able to study EUA or investigational mAbs with accessible sequences or structure information, and the conclusions may not be applicable to other EUA or investigational mAbs.

STAR★METHODS

Detailed methods are provided in the online version of this paper and include the following:

SUPPLEMENTAL INFORMATION

Supplemental information can be found online at https://doi.org/10.1016/j.immuni.2021.06.003.

ACKNOWLEDGMENTS

We acknowledge the work and contributions of all health care providers from Beijing Youan Hospital, Beijing Ditan Hospital, and Shenzhen Third People's Hospital. We also thank affected individuals for their active participation. This study was supported by the National Key Plan for Scientific Research and Development of China (2020YFC0848800 and 2020YFC0849900), the National Natural Science Foundation (81530065, 91442127, and 32000661), the Beijing Municipal Science and Technology Commission (D171100000517 and Z201100005420019), and the Science and Technology Innovation Committee of Shenzhen Municipality (202002073000002). It is also supported by funds from the COVID-19 Science and Technology Project of Beijing Hospitals Authority (YGZX-C1), the Beijing Advanced Innovation Center for Structural Biology, the Tsinghua University Scientific Research Program (20201080053 and 2020Z99CFG004), the Tencent Foundation, the Shuidi Foundation, the TH Capital and the National Science Fund for Distinguished Young Scholars (82025022), and the China Postdoctoral Science Foundation (2020T130062ZX). The funders had no role in study design, data collection, analysis, and interpretation or writing of the report. We thank the SSRF BL17U1 beamline for data collection and processing.

AUTHOR CONTRIBUTIONS

L.Z., X.W., and T.Z. conceived and designed the study. R.W., Q.Z., and J.G. performed most of the experiments with assistance from R.Z., J.L., and P.C. J.G. and J. L. produced the RBD and ACE2 recombinant proteins and solved and analyzed the crystal structure of the antibody-RBD complex. P.C. provided assistance with antibody production. W.R and Q.D. provided HeLa cell lines expressing ACE2 from diverse origins. T.Z., F.Z., Z.Z., and H.L. provided clinical care and management of infected individuals, particularly recruitment and following up of study subjects. T.Z., F.Z., Z.Z., B.J., B.S., F.Y., Y.F., X.L., and X.S. conducted sample collection, processing, and initial characterization. R.W., Q.Z., J.G., T.Z., X.W., and L.Z. had full access to the data in the study, generated figures and tables, and take responsibility for the integrity and accuracy of the data presentation. X.W. and L.Z. wrote the manuscript. All authors reviewed and approved the final version of the manuscript.

DECLARATION OF INTERESTS

Patent applications have been filed on monoclonal antibodies targeting SARS-CoV-2 (patent application number: PCT/CN2020/108718; patent applicants: The Third People's Hospital of Shenzhen and Tsinghua University). Q.Z., B.J., X.S., Z.Z., and L.Z. are the inventors. Q.Z., X.S., and L.Z. are shareholders of TSB Therapeutics.

Received: March 13, 2021
Revised: May 23, 2021
Accepted: June 4, 2021
Published: June 8, 2021

REFERENCES

Adams, P.D., Afonine, P.V., Bunkóczi, G., Chen, V.B., Davis, I.W., Echols, N., Headd, J.J., Hung, L.W., Kapral, G.J., Grosse-Kunstleve, R.W., et al. (2010). PHENIX: a comprehensive Python-based system for macromolecular structure solution. Acta crystallographica. Section D, Biological crystallography *66*, 213–221.

Baden, L.R., El Sahly, H.M., Essink, B., Kotloff, K., Frey, S., Novak, R., Diemert, D., Spector, S.A., Rouphael, N., Creech, C.B., et al.; COVE Study Group (2021). Efficacy and Safety of the mRNA-1273 SARS-CoV-2 Vaccine. N. Engl. J. Med. *384*, 403–416.

Barnes, C.O., Jette, C.A., Abernathy, M.E., Dam, K.A., Esswein, S.R., Gristick, H.B., Malyutin, A.G., Sharaf, N.G., Huey-Tubman, K.E., Lee, Y.E., et al. (2020). SARS-CoV-2 neutralizing antibody structures inform therapeutic strategies. Nature *588*, 682–687.

Callaway, E. (2021). Fast-spreading COVID variant can elude immune responses. Nature *589*, 500–501.

Cao, Y., Su, B., Guo, X., Sun, W., Deng, Y., Bao, L., Zhu, Q., Zhang, X., Zheng, Y., Geng, C., et al. (2020). Potent Neutralizing Antibodies against SARS-CoV-2 Identified by High-Throughput Single-Cell Sequencing of Convalescent Patients' B Cells. Cell *182*, 73–84.e16.

Cerutti, G., Guo, Y., Zhou, T., Gorman, J., Lee, M., Rapp, M., Reddem, E.R., Yu, J., Bahna, F., Bimela, J., et al. (2021). Potent SARS-CoV-2 neutralizing antibodies directed against spike N-terminal domain target a single supersite. Cell Host Microbe *29*, 819–833.e7.

Chan, K.K., Tan, T.J.C., Narayanan, K.K., and Procko, E. (2021). An engineered decoy receptor for SARS-CoV-2 broadly binds protein S sequence variants. Sci. Adv. Published online December 21, 2020. https://doi.org/10.1101/2020.10.18.344622.

Chen, P., Nirula, A., Heller, B., Gottlieb, R.L., Boscia, J., Morris, J., Huhn, G., Cardona, J., Mocherla, B., Stosor, V., et al.; BLAZE-1 Investigators (2021). SARS-CoV-2 Neutralizing Antibody LY-CoV555 in Outpatients with Covid-19. N. Engl. J. Med. *384*, 229–237.

Chi, X., Yan, R., Zhang, J., Zhang, G., Zhang, Y., Hao, M., Zhang, Z., Fan, P., Dong, Y., Yang, Y., et al. (2020). A neutralizing human antibody binds to the N-terminal domain of the Spike protein of SARS-CoV-2. Science *369*, 650–655.

Corbett, K.S., Flynn, B., Foulds, K.E., Francica, J.R., Boyoglu-Barnum, S., Werner, A.P., Flach, B., O'Connell, S., Bock, K.W., Minai, M., et al. (2020). Evaluation of the mRNA-1273 Vaccine against SARS-CoV-2 in Nonhuman Primates. N. Engl. J. Med. *383*, 1544–1555.

Diamond, M., Chen, R., Xie, X., Case, J., Zhang, X., VanBlargan, L., Liu, Y., Liu, J., Errico, J., Winkler, E., et al. (2021). SARS-CoV-2 variants show resistance to neutralization by many monoclonal and serum-derived polyclonal antibodies. Res. Sq, rs.3.rs-228079.

Du, S., Cao, Y., Zhu, Q., Yu, P., Qi, F., Wang, G., Du, X., Bao, L., Deng, W., Zhu, H., et al. (2020). Structurally Resolved SARS-CoV-2 Antibody Shows High Efficacy in Severely Infected Hamsters and Provides a Potent Cocktail Pairing Strategy. Cell *183*, 1013–1023.e13.

Emsley, P., Lohkamp, B., Scott, W.G., and Cowtan, K. (2010). Features and development of Coot. Acta crystallographica. Section D, Biological crystallography *66*, 486–501.

FDA (2021). Coronavirus Disease 2019 (COVID-19) (EUA Information).

Fujino, T., Nomoto, H., Kutsuna, S., Ujiie, M., Suzuki, T., Sato, R., Fujimoto, T., Kuroda, M., Wakita, T., and Ohmagari, N. (2021). Novel SARS-CoV-2 Variant Identified in Travelers from Brazil to Japan. Emerg. Infect. Dis. *27*, 1243–1245.

Ge, J., Wang, R., Ju, B., Zhang, Q., Sun, J., Chen, P., Zhang, S., Tian, Y., Shan, S., Cheng, L., et al. (2021). Antibody neutralization of SARS-CoV-2 through ACE2 receptor mimicry. Nat. Commun. *12*, 250.

GISAID (2021). COVID-19 Viral Genome Analysis Pipeline, https://cov.lanl.gov/content/index.

Gottlieb, R.L., Nirula, A., Chen, P., Boscia, J., Heller, B., Morris, J., Huhn, G., Cardona, J., Mocherla, B., Stosor, V., et al. (2021). Effect of Bamlanivimab as Monotherapy or in Combination With Etesevimab on Viral Load in Patients With Mild to Moderate COVID-19: A Randomized Clinical Trial. JAMA *325*, 632–644.

Hansen, J., Baum, A., Pascal, K.E., Russo, V., Giordano, S., Wloga, E., Fulton, B.O., Yan, Y., Koon, K., Patel, K., et al. (2020). Studies in humanized mice and convalescent humans yield a SARS-CoV-2 antibody cocktail. Science *369*, 1010–1014.

Hoffmann, M., Arora, P., Groß, R., Seidel, A., Hörnich, B.F., Hahn, A.S., Krüger, N., Graichen, L., Hofmann-Winkler, H., Kempf, A., et al. (2021). SARS-CoV-2 variants B.1.351 and P.1 escape from neutralizing antibodies. Cell *184*, 2384–2393.e12.

Hou, Y.J., Chiba, S., Halfmann, P., Ehre, C., Kuroda, M., Dinnon, K.H., 3rd, Leist, S.R., Schäfer, A., Nakajima, N., Takahashi, K., et al. (2020). SARS-CoV-2 D614G variant exhibits efficient replication ex vivo and transmission in vivo. Science *370*, 1464–1468.

Huang, B., Dai, L., Wang, H., Hu, Z., Yang, X., Tan, W., and Gao, G.F. (2021). Serum sample neutralisation of BBIBP-CorV and ZF2001 vaccines to SARS-CoV-2 501Y.V2. Lancet Microbe. Published online April 13, 2021. https://doi.org/10.1016/S2666-5247(21)00082-3.

Janson, G., Zhang, C., Prado, M.G., and Paiardini, A. (2017). PyMod 2.0: improvements in protein sequence-structure analysis and homology modeling within PyMOL. Bioinformatics *33*, 444–446.

Johnson & Johnson. (2021). Johnson & Johnson COVID-19 Vaccine Authorized by U.S. FDA For Emergency Use - First Single-Shot Vaccine in Fight Against Global Pandemic. https://www.prnewswire.com/news-releases/johnson–johnson-covid-19-vaccine-authorized-by-us-fda-for-emergency-use-301236878.html.

Ju, B., Zhang, Q., Ge, J., Wang, R., Sun, J., Ge, X., Yu, J., Shan, S., Zhou, B., Song, S., et al. (2020). Human neutralizing antibodies elicited by SARS-CoV-2 infection. Nature *584*, 115–119.

Korber, B., Fischer, W.M., Gnanakaran, S., Yoon, H., Theiler, J., Abfalterer, W., Hengartner, N., Giorgi, E.E., Bhattacharya, T., Foley, B., et al.; Sheffield COVID-19 Genomics Group (2020). Tracking Changes in SARS-CoV-2 Spike: Evidence that D614G Increases Infectivity of the COVID-19 Virus. Cell *182*, 812–827.e19.

Kreye, J., Reincke, S.M., Kornau, H.C., Sánchez-Sendin, E., Corman, V.M., Liu, H., Yuan, M., Wu, N.C., Zhu, X., Lee, C.D., et al. (2020). A Therapeutic Non-self-reactive SARS-CoV-2 Antibody Protects from Lung Pathology in a COVID-19 Hamster Model. Cell *183*, 1058–1069.e19.

Kupferschmidt, K. (2021). Fast-spreading U.K. virus variant raises alarms. Science *371*, 9–10.

Laffeber, C., de Koning, K., Kanaar, R., and Lebbink, J.H.G. (2021). Experimental Evidence for Enhanced Receptor Binding by Rapidly Spreading SARS-CoV-2 Variants. Journal of molecular biology *433*, 167058.

Lan, J., Ge, J., Yu, J., Shan, S., Zhou, H., Fan, S., Zhang, Q., Shi, X., Wang, Q., Zhang, L., and Wang, X. (2020). Structure of the SARS-CoV-2 spike receptor-binding domain bound to the ACE2 receptor. Nature *581*, 215–220.

Liu, L., Wang, P., Nair, M.S., Yu, J., Rapp, M., Wang, Q., Luo, Y., Chan, J.F., Sahi, V., Figueroa, A., et al. (2020). Potent neutralizing antibodies against multiple epitopes on SARS-CoV-2 spike. Nature *584*, 450–456.

Liu, Y., Hu, G., Wang, Y., Ren, W., Zhao, X., Ji, F., Zhu, Y., Feng, F., Gong, M., Ju, X., et al. (2021). Functional and genetic analysis of viral receptor ACE2

orthologs reveals a broad potential host range of SARS-CoV-2. Proc. Natl. Acad. Sci. USA *118*, e2025373118.

Maggi, F., Novazzi, F., Genoni, A., Baj, A., Spezia, P.G., Focosi, D., Zago, C., Colombo, A., Cassani, G., Pasciuta, R., et al. (2021). Imported SARS-COV-2 Variant P.1 Detected in Traveler Returning from Brazil to Italy. Emerg. Infect. Dis. *27*, 1249–1251.

McCallum, M., De Marco, A., Lempp, F.A., Tortorici, M.A., Pinto, D., Walls, A.C., Beltramello, M., Chen, A., Liu, Z., Zatta, F., et al. (2021). N-terminal domain antigenic mapping reveals a site of vulnerability for SARS-CoV-2. Cell *184*, 2332–2347.e2316.

McCoy, A.J., Grosse-Kunstleve, R.W., Adams, P.D., Winn, M.D., Storoni, L.C., and Read, R.J. (2007). Phaser crystallographic software. J. Appl. Cryst. *40*, 658–674.

Novavax (2021). Novavax COVID-19 Vaccine Demonstrates 89.3% Efficacy in UK Phase 3 Trial. https://ir.novavax.com/news-releases/news-release-details/novavax-covid-19-vaccine-demonstrates-893-efficacy-uk-phase-3.

Oude Munnink, B.B., Sikkema, R.S., Nieuwenhuijse, D.F., Molenaar, R.J., Munger, E., Molenkamp, R., van der Spek, A., Tolsma, P., Rietveld, A., Brouwer, M., et al. (2021). Transmission of SARS-CoV-2 on mink farms between humans and mink and back to humans. Science *371*, 172–177.

Pettersen, E.F., Goddard, T.D., Huang, C.C., Couch, G.S., Greenblatt, D.M., Meng, E.C., and Ferrin, T.E. (2004). UCSF Chimera–a visualization system for exploratory research and analysis. J. Comput. Chem. *25*, 1605–1612.

Pinto, D., Park, Y.J., Beltramello, M., Walls, A.C., Tortorici, M.A., Bianchi, S., Jaconi, S., Culap, K., Zatta, F., De Marco, A., et al. (2020). Cross-neutralization of SARS-CoV-2 by a human monoclonal SARS-CoV antibody. Nature *583*, 290–295.

Plante, J.A., Liu, Y., Liu, J., Xia, H., Johnson, B.A., Lokugamage, K.G., Zhang, X., Muruato, A.E., Zou, J., Fontes-Garfias, C.R., et al. (2021). Spike mutation D614G alters SARS-CoV-2 fitness. Nature *592*, 116–121.

Polack, F.P., Thomas, S.J., Kitchin, N., Absalon, J., Gurtman, A., Lockhart, S., Perez, J.L., Pérez Marc, G., Moreira, E.D., Zerbini, C., et al.; C4591001 Clinical Trial Group (2020). Safety and Efficacy of the BNT162b2 mRNA Covid-19 Vaccine. N. Engl. J. Med. *383*, 2603–2615.

Public Health England (2020). . Investigation of novel SARS-COV-2 variant: Variant of Concern 202012/01: technical briefings. https://www.gov.uk/government/publications/investigation-of-novel-sars-cov-2-variant-variant-of-concern-20201201.

Rambaut, A., Loman, N., Pybus, O., Barclay, W., Barrett, J., Carabelli, A., Connor, T., Peacock, T., Robertson, D.L., and Volz, E.; on behalf of the COVID-19 Genomics Consortium UK (CoG-UK) (2020). Preliminary genomic characterisation of an emergent SARS-CoV-2 lineage in the UK defined by a novel set of spike mutations. https://virological.org/t/preliminary-genomic-characterisation-of-an-emergent-sars-cov-2-lineage-in-the-uk-defined-by-a-novel-set-of-spike-mutations/563.

Rathnasinghe, R., Jangra, S., Cupic, A., Martínez-Romero, C., Mulder, L.C.F., Kehrer, T., Yildiz, S., Choi, A., Mena, I., De Vrieze, J., et al. (2021). The N501Y mutation in SARS-CoV-2 spike leads to morbidity in obese and aged mice and is neutralized by convalescent and post-vaccination human sera. medRxiv. https://doi.org/10.1101/2021.01.19.21249592.

Robbiani, D.F., Gaebler, C., Muecksch, F., Lorenzi, J.C.C., Wang, Z., Cho, A., Agudelo, M., Barnes, C.O., Gazumyan, A., Finkin, S., et al. (2020). Convergent antibody responses to SARS-CoV-2 in convalescent individuals. Nature *584*, 437–442.

Sabino, E.C., Buss, L.F., Carvalho, M.P.S., Prete, C.A., Jr., Crispim, M.A.E., Fraiji, N.A., Pereira, R.H.M., Parag, K.V., da Silva Peixoto, P., Kraemer, M.U.G., et al. (2021). Resurgence of COVID-19 in Manaus, Brazil, despite high seroprevalence. Lancet *397*, 452–455.

Shi, R., Shan, C., Duan, X., Chen, Z., Liu, P., Song, J., Song, T., Bi, X., Han, C., Wu, L., et al. (2020). A human neutralizing antibody targets the receptor-binding site of SARS-CoV-2. Nature *584*, 120–124.

Sun, S., Gu, H., Cao, L., Chen, Q., Yang, G., Li, R.-T., Fan, H., Ye, Q., Deng, Y.-Q., Song, X., et al. (2020). Characterization and structural basis of a lethal mouse-adapted SARS-CoV-2. bioRxiv. https://doi.org/10.1101/2020.11.10.377333.

Suryadevara, N., Shrihari, S., Gilchuk, P., VanBlargan, L.A., Binshtein, E., Zost, S.J., Nargi, R.S., Sutton, R.E., Winkler, E.S., Chen, E.C., et al. (2021). Neutralizing and protective human monoclonal antibodies recognizing the N-terminal domain of the SARS-CoV-2 spike protein. Cell *184*, 2316–2331.e15.

Tegally, H., Wilkinson, E., Lessells, R.J., Giandhari, J., Pillay, S., Msomi, N., Mlisana, K., Bhiman, J.N., von Gottberg, A., Walaza, S., et al. (2021). Sixteen novel lineages of SARS-CoV-2 in South Africa. Nat. Med. *27*, 440–446.

Tian, F., Tong, B., Sun, L., Shi, S., Zheng, B., Wang, Z., Dong, X., and Zheng, P. (2021). Mutation N501Y in RBD of Spike Protein Strengthens the Interaction between COVID-19 and its Receptor ACE2. bioRxiv. https://doi.org/10.1101/2021.02.14.431117.

Vogel, A.B., Kanevsky, I., Che, Y., Swanson, K.A., Muik, A., Vormehr, M., Kranz, L.M., Walzer, K.C., Hein, S., Guler, A., et al. (2021). BNT162b vaccines protect rhesus macaques from SARS-CoV-2. Nature *592*, 283–289.

Volz, E., Hill, V., McCrone, J.T., Price, A., Jorgensen, D., O'Toole, Á., Southgate, J., Johnson, R., Jackson, B., Nascimento, F.F., et al.; COG-UK Consortium (2021). Evaluating the Effects of SARS-CoV-2 Spike Mutation D614G on Transmissibility and Pathogenicity. Cell *184*, 64–75.e11.

Voysey, M., Clemens, S.A.C., Madhi, S.A., Weckx, L.Y., Folegatti, P.M., Aley, P.K., Angus, B., Baillie, V.L., Barnabas, S.L., Bhorat, Q.E., et al.; Oxford COVID Vaccine Trial Group (2021). Safety and efficacy of the ChAdOx1 nCoV-19 vaccine (AZD1222) against SARS-CoV-2: an interim analysis of four randomised controlled trials in Brazil, South Africa, and the UK. Lancet *397*, 99–111.

Wang, H., Zhang, Y., Huang, B., Deng, W., Quan, Y., Wang, W., Xu, W., Zhao, Y., Li, N., Zhang, J., et al. (2020). Development of an Inactivated Vaccine Candidate, BBIBP-CorV, with Potent Protection against SARS-CoV-2. Cell *182*, 713–721.e9.

Wang, P., Nair, M.S., Liu, L., Iketani, S., Luo, Y., Guo, Y., Wang, M., Yu, J., Zhang, B., Kwong, P.D., et al. (2021a). Antibody resistance of SARS-CoV-2 variants B.1.351 and B.1.1.7. Nature *593*, 130–135.

Wang, Z., Schmidt, F., Weisblum, Y., Muecksch, F., Barnes, C.O., Finkin, S., Schaefer-Babajew, D., Cipolla, M., Gaebler, C., Lieberman, J.A., et al. (2021b). mRNA vaccine-elicited antibodies to SARS-CoV-2 and circulating variants. Nature *592*, 616–622.

Weinreich, D.M., Sivapalasingam, S., Norton, T., Ali, S., Gao, H., Bhore, R., Musser, B.J., Soo, Y., Rofail, D., Im, J., et al.; Trial Investigators (2021). REGN-COV2, a Neutralizing Antibody Cocktail, in Outpatients with Covid-19. N. Engl. J. Med. *384*, 238–251.

Weissman, D., Alameh, M.G., de Silva, T., Collini, P., Hornsby, H., Brown, R., LaBranche, C.C., Edwards, R.J., Sutherland, L., Santra, S., et al. (2021). D614G Spike Mutation Increases SARS CoV-2 Susceptibility to Neutralization. Cell Host Microbe *29*, 23–31.e4.

Wu, K., Werner, A.P., Koch, M., Choi, A., Narayanan, E., Stewart-Jones, G.B.E., Colpitts, T., Bennett, H., Boyoglu-Barnum, S., Shi, W., et al. (2021). Serum Neutralizing Activity Elicited by mRNA-1273 Vaccine. N. Engl. J. Med. *384*, 1468–1470.

Wu, S., Zhong, G., Zhang, J., Shuai, L., Zhang, Z., Wen, Z., Wang, B., Zhao, Z., Song, X., Chen, Y., et al. (2020). A single dose of an adenovirus-vectored vaccine provides protection against SARS-CoV-2 challenge. Nat. Commun. *11*, 4081.

Xia, S., Zhang, Y., Wang, Y., Wang, H., Yang, Y., Gao, G.F., Tan, W., Wu, G., Xu, M., Lou, Z., et al. (2021). Safety and immunogenicity of an inactivated SARS-CoV-2 vaccine, BBIBP-CorV: a randomised, double-blind, placebo-controlled, phase 1/2 trial. Lancet Infect. Dis. *21*, 39–51.

Yu, F., Wang, Q., Li, M., Zhou, H., Liu, K., Zhang, K., Wang, Z., Xu, Q., Xu, C., Pan, Q., and He, J. (2019). Aquarium: an automatic data-processing and experiment information management system for biological macromolecular crystallography beamlines. J. Appl. Cryst. *52*, 472–477.

Yuan, M., Liu, H., Wu, N.C., Lee, C.D., Zhu, X., Zhao, F., Huang, D., Yu, W., Hua, Y., Tien, H., et al. (2020a). Structural basis of a shared antibody response to SARS-CoV-2. Science *369*, 1119–1123.

Yuan, M., Wu, N.C., Zhu, X., Lee, C.D., So, R.T.Y., Lv, H., Mok, C.K.P., and Wilson, I.A. (2020b). A highly conserved cryptic epitope in the receptor binding domains of SARS-CoV-2 and SARS-CoV. Science *368*, 630–633.

Yuan, M., Huang, D., Lee, C.D., Wu, N.C., Jackson, A.M., Zhu, X., Liu, H., Peng, L., van Gils, M.J., Sanders, R.W., et al. (2021). Structural and functional ramifications of antigenic drift in recent SARS-CoV-2 variants. Science, eabh1139.

Yurkovetskiy, L., Wang, X., Pascal, K.E., Tomkins-Tinch, C., Nyalile, T.P., Wang, Y., Baum, A., Diehl, W.E., Dauphin, A., Carbone, C., et al. (2020). Structural and Functional Analysis of the D614G SARS-CoV-2 Spike Protein Variant. Cell *183*, 739–751.e8.

Zhou, P., Yang, X.L., Wang, X.G., Hu, B., Zhang, L., Zhang, W., Si, H.R., Zhu, Y., Li, B., Huang, C.L., et al. (2020). A pneumonia outbreak associated with a new coronavirus of probable bat origin. Nature *579*, 270–273.

Zost, S.J., Gilchuk, P., Case, J.B., Binshtein, E., Chen, R.E., Nkolola, J.P., Schäfer, A., Reidy, J.X., Trivette, A., Nargi, R.S., et al. (2020). Potently neutralizing and protective human antibodies against SARS-CoV-2. Nature *584*, 443–449.

STAR★METHODS

KEY RESOURCES TABLE

REAGENT or RESOURCE	SOURCE	IDENTIFIER
Antibodies		
P2C-1F11	Ju et al., 2020	N/A
P5A-1D2	Ju et al., 2020	N/A
P5A-3C8	Ju et al., 2020	N/A
P22A-1D1	Ju et al., 2020	N/A
P5A-1B9	Ju et al., 2020	N/A
P2B-1G5	Ju et al., 2020	N/A
REGN10933	Hansen et al., 2020	N/A
REGN10987	Hansen et al., 2020	N/A
CB6	Shi et al., 2020	N/A
S309	Pinto et al., 2020	N/A
4A8	Chi et al., 2020	N/A
CR3022	Yuan et al., 2020b	N/A
Anti-coronavirus (SARS-CoV-2) spike S2 mouse mAb	MP Biomedicals	Cat#08720401
PE anti-human IgG Fc	Biolegend	Cat#410708
Goat anti-Mouse IgG (H+L) Cross-Adsorbed Secondary Antibody, FITC	Invitrogen	Cat#A16073
PE anti-his tag	Biolegend	Cat#362603
Bacterial and virus strains		
SARS-CoV-2/WH-09/human/2020/CHN	GenBank	MN908947.3
SARS-CoV-2/UK B.1.1.7	GISAID	EPI_ISL_601443
SARS-CoV-2/SA B.1.351	GISAID	EPI_ISL_700450
SARS-CoV-2/BR P.1	GISAID	EPI_ISL_792681
Per site variation v20210517	GISAID	https://cov.lanl.gov/content/index
Biological samples		
International Standard for anti-SARS-CoV-2 immunoglobulin	NISBIC	Cat#20/136
23 plasma samples from convalescent patients	This paper	N/A
Chemicals, peptides, and recombinant proteins		
Polyethyleneimine	Polysciences	Cat#24765-1
Endoproteinase Lys-C	Roche	Cat#11047825001
Trypsin	Macgene	Cat#CC017
Fetal bovine serum	GIBCO	Cat#16000-044
ACE2 recombinant protein	This paper	Lan et al., 2020
Recombinant wildtype RBD	This paper	Lan et al., 2020
Recombinant RBD with 417N/484K/501Y mutations	This paper	N/A
Cellfectin II Reagents	GIBCO	Cat#10362100
Recombinant protein A	Sino Biological	Cat#10600-P07E
His capture kit	Cytiva	Cat#28-9950-56
Critical commercial assays		
QuikChange Lightning Site-Directed Mutagenesis Kit	Agilent	Cat#210519

(*Continued on next page*)

Continued		
REAGENT or RESOURCE	SOURCE	IDENTIFIER
Bright-Glo™ Luciferase Assay Buffer	Promega	Cat#E264B
Bright-Glo™ Luciferase Assay Substrate	Promega	Cat#E263B
Deposited data		
P2C-1F11 with mutated RBD structure	This paper	PDB: 7E8M
Experimental models: cell lines		
Human: HEK293T, embryo	ATCC	CRL-3216
Human: FreeStyle 293F, embryo	Thermo Fisher	R79007
Human: Huh-7, Male	JCRB	JCRB0403
Human:HeLa, Female	ATCC	CCL-2
HeLa expressing ACE2 from diverse origin, Female	Dr. Qiang Ding's lab	Liu et al., 2021
Sf9 cells, Female	ATCC	CRL-3357
Recombinant DNA		
pcDNA3.1	Thermo Fisher	Cat#V79020
pLVX-IRES-zsGreen1 vector	Clontech Laboratories, Inc	Cat#632187
pFastBac-Dual vector	GIBCO	Cat#10712024
pNL4-3- luc -R-E	NIH-AIDS Reagent Program	Cat#3418
Software and algorithms		
Graphpad Prism 7	GraphPad	www.graphpad.com
Microsoft Excel	Microsoft	www.microsoft.com
FlowJo 10 software	FlowJo	https://www.flowjo.com/
Biacore Insight Evaluation Software	GE Healthcare	https://www.cytivalifesciences.com/en/us/shop/protein-analysis/spr-label-free-analysis/software/biacore-insight-evaluation-software-p-23528
PHASER (CCP4 Program Suite)	McCoy et al., 2007	http://www.phaser.cimr.cam.ac.uk/index.php/Phaser_Crystallographic_Software
COOT	Emsley et al., 2010	http://www2.mrc-lmb.cam.ac.uk/Personal/pemsley/coot/
PHENIX	Adams et al., 2010	http://www.phenix-online.org/
PyMOL	Janson et al., 2017	https://pymol.org/2/
Chimera	Pettersen et al., 2004	https://www.cgl.ucsf.edu/chimera/
Other		
Superdex 200 High-Performance column	GE Healthcare	N/A
Nanodrop 2000 Spectrophotometer	Thermo Scientific	N/A
BD LSRFortassa	BD Biosciences	N/A
CM5 sensor chip	GE Healthcare	Cat#BR100530
Biacore 8K	GE Healthcare	N/A

RESOURCE AVAILABILITY

Lead contact

Further information and requests for resources and primary data should be directed to and will be fulfilled by the Lead Contact, Linqi Zhang (Zhanglinqi@mail.tsinghua.edu.cn).

Materials availability

There are restrictions to the availability of convalescent plasma due to limited stock. We will share these reagents until the stock runs out.

Data and code availability

The coordinates and structure factors files for P2C-1F11 and RBD-3M complex have been deposited to the Protein Data Bank (http://www.rcsb.org) with accession code 7E8M.

EXPERIMENTAL MODEL AND SUBJECT DETAILS

Study approval

This study received approval from the Research Ethics Committee of Beijing Youan Hospital (LL-2020-039-K), Beijing Ditan Hospital (2020-019-01), and Shenzhen Third People's Hospital (2020-084). The research was conducted in strict accordance with the rules and regulations of the Chinse government for the protection of human subjects. The study subjects agreed and signed the written informed consents for research use of their blood samples.

Human samples

The study enrolled a total of 23 convalescent patients aged from 29 to 81 years old, with an average of 56, infected with SARS-CoV-2 between January to February 2020. SARS-CoV-2 infection status was verified by RT-PCR of nasopharyngeal swab and chest computed tomographic scan. Of the 23 infected individuals, thirteen were males and ten were females. Fourteen individuals developed only mild symptom and the remaining nine developed severe pneumonia. The specific information is provided in Table S3. Convalescent blood samples were collected during hospitalization or follow-up visits in Beijing Youan Hospital, Beijing Ditan Hospital, or Shenzhen Third People's Hospital, within two months after symptom onset. A blood sample from a healthy control individual was also included. Blood samples were separated into plasma and peripheral blood mononuclear cells (PBMC) by Ficoll-Hypaque gradient (GE Healthcare) centrifugation. All plasma samples were heat-inactivated at 56°C for 1h before being stored at −80°C. PBMCs were maintained in freezing media and stored in liquid nitrogen until use.

Cell lines

HEK293T cells (ATCC, CRL-3216), Huh7 cells (JCRB, JCRB0403), HeLa cells (ATCC, CCL-2) and HeLa cells expressing ACE2 orthologs (kindly provided by Dr. Qiang Ding) were maintained at 37°C in 5% CO2 in Dulbecco's minimal essential medium (DMEM) containing 10% (v/v) heat-inactivated fetal bovine serum (FBS) and 100 U/mL of penicillin–streptomycin. FreeStyle 293F cells (Thermo Fisher Scientific, R79007) were maintained at 37°C in 8% CO2. Sf9 cells (ATCC, CRL-3357) were maintained at 27°C in Sf-900 II SFM medium.

METHOD DETAILS

Production of mAbs and Fab

P2C-1F11, P5A-1D2, P5A-3C8, P22A-1D2, P5A-1B9 and P2B-1G5 are potent neutralizing mAbs initially isolated from SARS-CoV-2 infected patients by our group and previously published (Ju et al., 2020). BRII-196 and BRII-198 are Fc-modified version of P2C-1F11 and P2B-1G5, respectively, which are being investigated in the phase III clinical trial. Antibodies published by other groups including REGN10933, REGN10987, CB6, S309, 4A8 and CR3022 were synthesized according to the sequences released in Protein Data Bank (PDB) (Chi et al., 2020; Hansen et al., 2020; Pinto et al., 2020; Shi et al., 2020; Yuan et al., 2020b). Antibody production was conducted by co-transfection of the heavy and light chain expression vectors into HEK293F cells using polyethyleneimine (PEI)(Polysciences). After 96h, antibodies secreted into the supernatant were captured by Protein A-Sepharose (GE Healthcare) and eluted by solution buffer Glycine pH 3.0. After further purification by gel-filtration chromatography with Superdex 200 High-Performance column (GE Healthcare), antibody concentration was determined by nanodrop 2000 Spectrophotometer (Thermo Scientific). To produce Fab fragment, purified P2C-1F11 were cleaved using Endoproteinase Lys-C (Roche) with IgG to Lys-C ratio of 4000:1 (w/w) in 10 mM EDTA, 100 mM Tris-HCl, pH 8.5 at 37°C overnight. Fc fragment were removed using Protein A-Sepharose.

Production of SARS-CoV-2 wild-type and variant pseudoviruses

The wild-type pseudovirus used throughout the analysis was the prototype strain (GenBank: MN908947.3) with a D614G mutation (WT D614G). The variant B.1.1.7 (GISAID: EPI_ISL_601443) was constructed with total of 9 mutations including 69-70del, 144del, N501Y, A570D, D614G, P681H, T716I, S982A and D1118H. The variant B.1.351 (GISAID: EPI_ISL_700450) was constructed with 10 mutations including L18F, D80A, D215G, 242-244del, S305T, K417N, E484K, N501Y, D614G and A701V. The variant P.1 (GISAID: EPI_ISL_792681) was constructed with 12 mutations including L18F, T20N, P26S, D138Y, R190S, K417T, E484K, N501Y, D614G, H655Y, T1027I and V1176F. The gene of variants were synthesized In Genwiz, Inc. The single mutations identified from the GISAID database were introduced into the pcDNA3.1 vector encoding WT D614G using QuickChange site-directed mutagenesis (Agilent 210519). SARS-CoV-2 pseudoviruses were generated by co-transfecting HEK293T cells (ATCC) with human immunodeficiency virus backbones expressing firefly luciferase (pNL4-3-R-E-luciferase) and pcDNA3.1 vector encoding either wild-type or mutated S proteins. Viral supernatant was collected 48h or 72h later, centrifuged to remove cell lysis, and stored at −80°C until use.

HeLa cell lines expressing ACE2 from diverse origin

HeLa cells expressing ACE2 orthologs were kindly provided by Dr. Qiang Ding at Tsinghua University School of Medicine. The species names and accession numbers for the ACE2 orthologs used are as follows: Human, *Homo sapiens*, NP_001358344.1; Rsbat, Rhinolophus sinicus, KC881004.1; Erbat, Rousettus aegyptiacus, XP_015974412.1; Pangolin, Manis javanica, XP_017505746.1; Pig, Sus scrofa, NP_001116542.1; Cat, Felis catus, XP_023104564.1; Dog, Canis lupus familiaris, NP_001158732.1; Mink, Mustela lutreola, MT560518.1; Mouse, *Mus musculus*, NP_001123985.1. The cDNAs encoding ACE2 orthologs were synthesized by GenScript and cloned into pLVX-IRES-zsGreen1 vectors (Catalog No. 632187, Clontech Laboratories, Inc) with a C-terminal FLAG tag. VSV-G pseudotyped lentiviruses expressing ACE2 orthologs were produced and used to generate HeLa-ACE2 cells as previously described (Liu et al., 2021). For studying entry efficiency of SARS-CoV-2 variants, HeLa-ACE2 cells were added to 96 well plates, mixed with 50 ul of pseudovirus, and analyzed the luciferase activities 60 h after infection using Bright-Glo Luciferase Assay Vector System (Promega Bioscience). Absolute and fold changes between mutated and WT D614G were used to estimate the entry efficiency of SARS-CoV-2 variants.

mAbs and plasma neutralization using pseudoviruses

Serial dilutions of mAbs were prepared with the highest concentration of 1 μg/ml except for S309 and P2B-1G5 (10 μg/ml). Serial dilutions of convalescent plasma were prepared with the highest dilution of 1:60 except for P#2, P#5, P#22 and International Standard for anti-SARS-CoV-2 immunoglobulin (human) (NIBSC code: 20/136) where 1:200 was the initial dilution. Wild-type or mutated spike pseudovirus were mixed with mAbs or plasma and incubated at 37°C for 1h. HeLa-ACE2 cells (except for S309 where Huh7 cell was used) were then added into the mixture and incubated at 37°C for 60h before cell lysis for measuring luciferase-activity. The percent of neutralization was determined by comparing with the virus control.

Binding of mAb and ACE2 to cell surface-expressed wild-type and mutated S glycoprotein

The entire procedure was conducted as previously published (Ge et al., 2021). Specifically, HEK293T cells were transfected with expression plasmids encoding either wild-type or mutated SARS-CoV-2 S glycoproteins, and incubated at 37°C for 36 h. Cells were digested from the plate with trypsin and distributed onto 96-well plates. Cells were washed twice with 200 μL staining buffer (PBS with 2% heated-inactivated fetal bovine serum (FBS)) between each of the following steps. First, cells were stained with the testing mAb, S2-specific monoclonal antibody (MP Biomedicals, Singapore 08720401), or ACE2 recombinant protein at 4°C for 30 min in 100 μL staining buffer. Then, PE-labeled anti-human IgG Fc (Biolegend 410718), anti-mouse IgG FITC (ThermoFisher Scientific A10673), or anti-his PE secondary antibody (Miltenyi 130120787) was added in 40 μL staining buffer at 4°C for 30 min. After extensive washes, the cells were resuspended and analyzed with BD LSRFortassa (BD Biosciences, USA) and FlowJo 10 software (FlowJo, USA). The serial dilution of concentration of mAbs and ACE2 were tested and the lowest saturated concentrations were used in the assay (2 μg/ml for ACE2, 0.1 μg/ml for all mAbs except for P2B-1G5 and CR3022 where 2 μg/ml was used). HEK293T cells with mock transfection were stained as background control. Antibody binding percentages were calculated by the ratio between mutated over wild-type MFI normalized in relative to that of S2 specific antibody. All MFI values were weighted by multiplying the number of positive cells in the selected gates.

Recombinant RBD and ACE2 protein

Recombinant wild-type RBD, RBD with 417N-484K-501Y mutations, and human receptor ACE2 peptidase domain were expressed using the Bac-to-Bac Baculovirus System (Invitrogen) as previously described (Lan et al., 2020). Specifically, SARS-CoV-2 RBD (residues Arg319 to Lys529) or ACE2 (residues Ser19 to Asp615) containing the gp67 secretion signal peptide and a C-terminal hexahistidine was inserted into pFastBac-Dual vectors (Invitrogen) and transformed into DH10 Bac component cells. The recombinant bacmid was extracted and further transfected into Sf9 cells using Cellfectin II Reagents (Invitrogen). The recombinant viruses were harvested from the transfected supernatant and amplified to generate high-titer virus stock. Viruses were then used to infect Sf9 cells for protein expression. Secreted RBD and ACE2 were harvested from the supernatant, captured by Ni-NTA Sepharose (GE Healthcare) and purified by gel filtration chromatography.

Antibody binding kinetics measured by SPR

The binding kinetics of IgG or Fab form of mAbs to SARS-CoV-2 RBD or mutated RBD were analyzed by SPR (Biacore 8K, GE Healthcare). Specifically, recombinant protein A (Sino Biological) or anti-his antibody (Cytiva) were covalently immobilized to a CM5 sensor chip via amine groups in 10 mM sodium acetate buffer (pH 4.5) for a final RU around 7000. The running buffer was composed of 10mM PBS, pH 7.2 and 0.05% Tween 20. For IgG form, diverse IgG form of mAbs were captured by the sensor chip immobilized with recombinant protein A and then Serial dilutions of wild-type and mutated SARS-CoV-2 RBDs flowed through the sensor chip system. For Fab form, wild-type and mutated SARS-CoV-2 RBDs were captured by the sensor chip immobilized with anti-his antibody and then dilutions of P2C-1F11 Fab flowed through the sensor chip system. The resulting data were fitted to a 1:1 binding model using Biacore Evaluation Software (GE Healthcare).

Crystal analysis and data collection

P2C-1F11 Fab fragments were mixed with SARS-CoV-2 RBD containing K417N-E484K-N501Y mutations at a molar ratio of 1:1.2, incubated on ice for 2 h, and further purified by gel-filtration chromatography. The purified complex was concentrated to 11 mg/mL in

HBS buffer (10 mM HEPES, pH 7.2, 150 mM NaCl) for crystallization. Screening trials were performed at 18°C. The sitting drop vapor diffusion method was used by mixing 0.2 μL of protein with 0.2 μL of reservoir solution. Crystals of RBD–Fab complexes were successfully obtained in 0.2 M Ammonium sulfate, 0.1M Tris 8.5, 12% w/v PEG 8000. Diffraction data were collected at the BL17U1 beamline of the Shanghai Synchrotron Research Facility (SSRF) and auto-processed with aquarium pipeline (Yu et al., 2019).

Structural determination and refinement

Structures were determined by the molecular replacement method using PHASER (CCP4 Program Suite) (McCoy et al., 2007). Search models were the SARS-CoV-2 RBD structure (PDB: 6M0J) and the heavy and light chain variable domain structures available in the PDB with the highest sequence identities. Subsequent model building and refinement were performed using COOT and PHENIX, respectively (Adams et al., 2010; Emsley et al., 2010). All structural figures were generated using PyMOL and Chimera (Janson et al., 2017; Pettersen et al., 2004).

QUANTIFICATION AND STATISTICAL ANALYSIS

The technical and independent experiment replicates were indicated in the figure legends. Half-maximal inhibitory concentration (IC_{50}) of mAb or dilutions (ID50) of convalescent plasmas were calculated by the equation of four-parameter dose inhibition response using Graphpad Prism 7.0. The fold change of mutant S relative to WT D614G in binding or neutralization were calculated by simple division of respective IC_{50} or ID50 values. The overall fold change of mutant pseudovirus relative to WT D614G in neutralization of convalescent plasma was calculated by the comparison of geometric mean of the ID50 value of the 23 plasma samples. The significance of neutralizing activities of convalescent plasma against each mutant pseudovirus relative to D614G was estimated using the unpaired Mann-Whiteny t test by Graphpad Prism 7 (n = 23).

Immunity, Volume *54*

Supplemental information

Analysis of SARS-CoV-2 variant mutations reveals neutralization escape mechanisms and the ability to use ACE2 receptors from additional species

Ruoke Wang, Qi Zhang, Jiwan Ge, Wenlin Ren, Rui Zhang, Jun Lan, Bin Ju, Bin Su, Fengting Yu, Peng Chen, Huiyu Liao, Yingmei Feng, Xuemei Li, Xuanling Shi, Zheng Zhang, Fujie Zhang, Qiang Ding, Tong Zhang, Xinquan Wang, and Linqi Zhang

Supplemental Information titles and legends

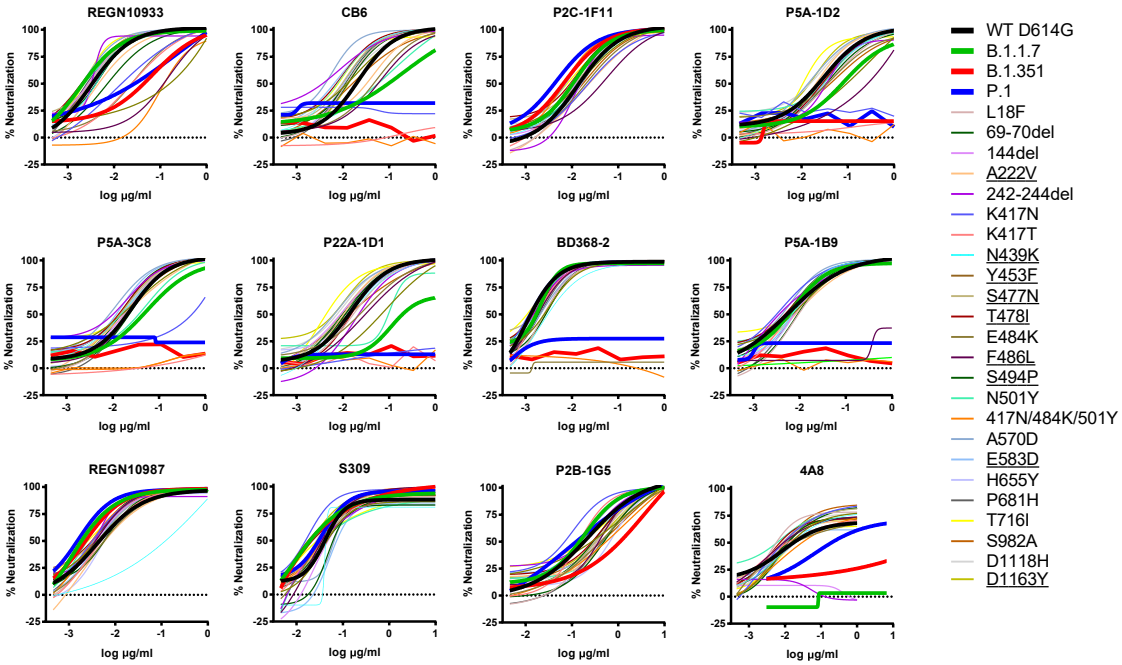

Figure S1.

Neutralization of SARS-CoV-2 variants by each antibody, related to Figure 1. Pseudoviruses bearing the indicated mutations were tested against serial dilutions of each mAb. Neutralizing activity was defined as the percent reduction in luciferase activities compared to no antibody controls. Levels of resistance were calculated as the -fold change in IC50 between each mutant and WT D614G, as presented in Figure 1C. Results were calculated from three independent experiments.

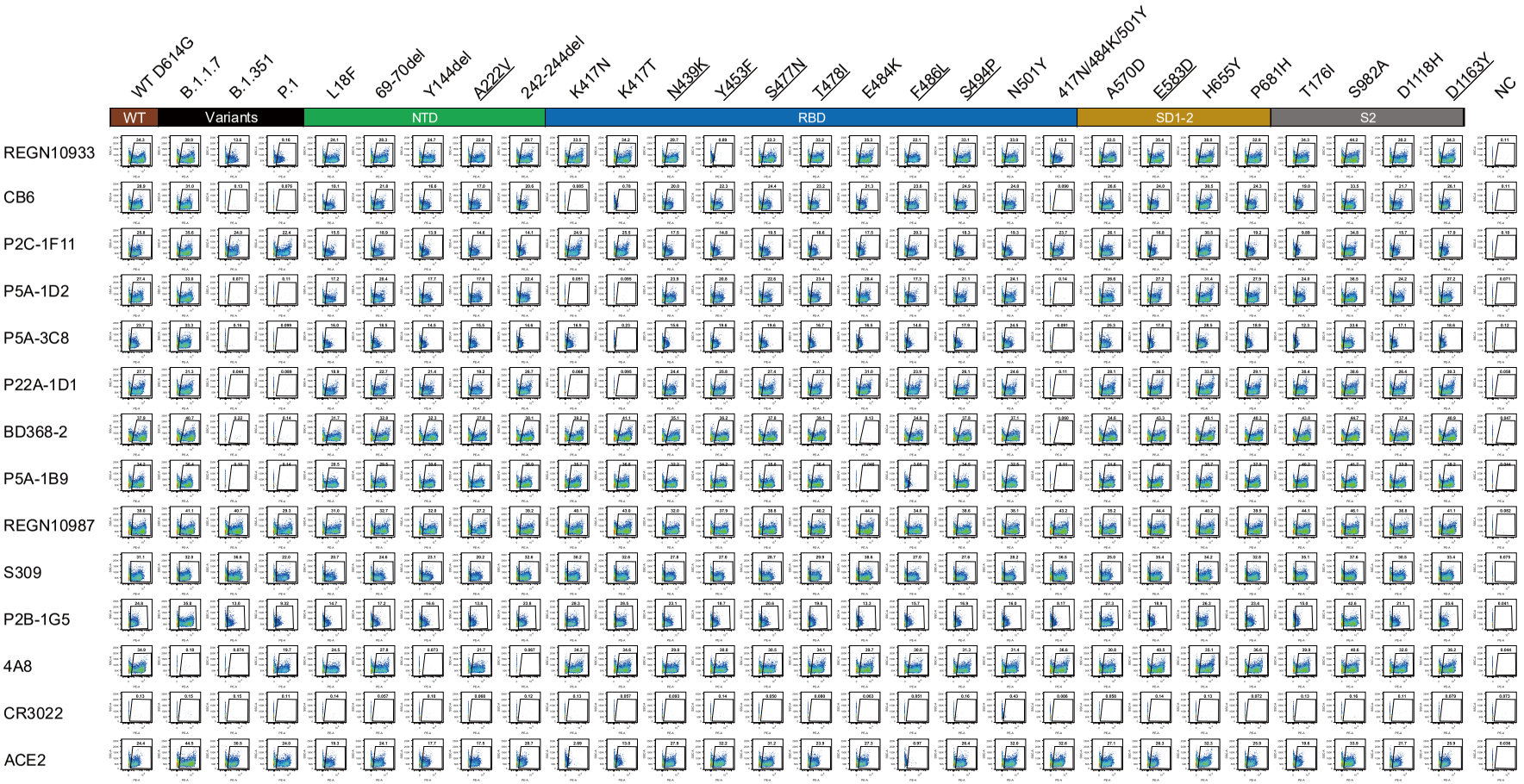
WT D614G
B.1.1.7
B.1.351
P.1
L18F
69-70del
Y144del
A222V
242-244del
K417N
K417T
N439K
Y453F
S477N
T478I
E484K
F486L
S494P
N501Y
417N/484K/501Y
A570D
E583D
H655Y
P681H
T176I
S982A
D1118H
D1163Y
NC
WT
Variants
NTD
RBD
SD1-2
S2
REGN10933
CB6
P2C-1F11
P5A-1D2
P5A-3C8
P22A-1D1
BD368-2
P5A-1B9
REGN10987
S309
P2B-1G5
4A8
CR3022
ACE2

Figure S2.

Binding to cell surface expressed SARS-CoV-2 variants by each antibody, related to Figure 1. Wildtype and mutant S proteins were expressed on the surface of HEK 293T, incubated with the mAbs or human soluble ACE2 under study, followed by staining with anti-human IgG Fc PE or anti-his PE, and analyzed by FACS. The gated cell percentages are shown. The fold changes in antibody binding, as shown in Figure 1D, was determined by comparing the total MFI in the selected gate between S variants and WT D614G. Data shown were calculated from three independent experiments. CR3022 is a negative control antibody. NC is HEK 293T cells with mock transfection.

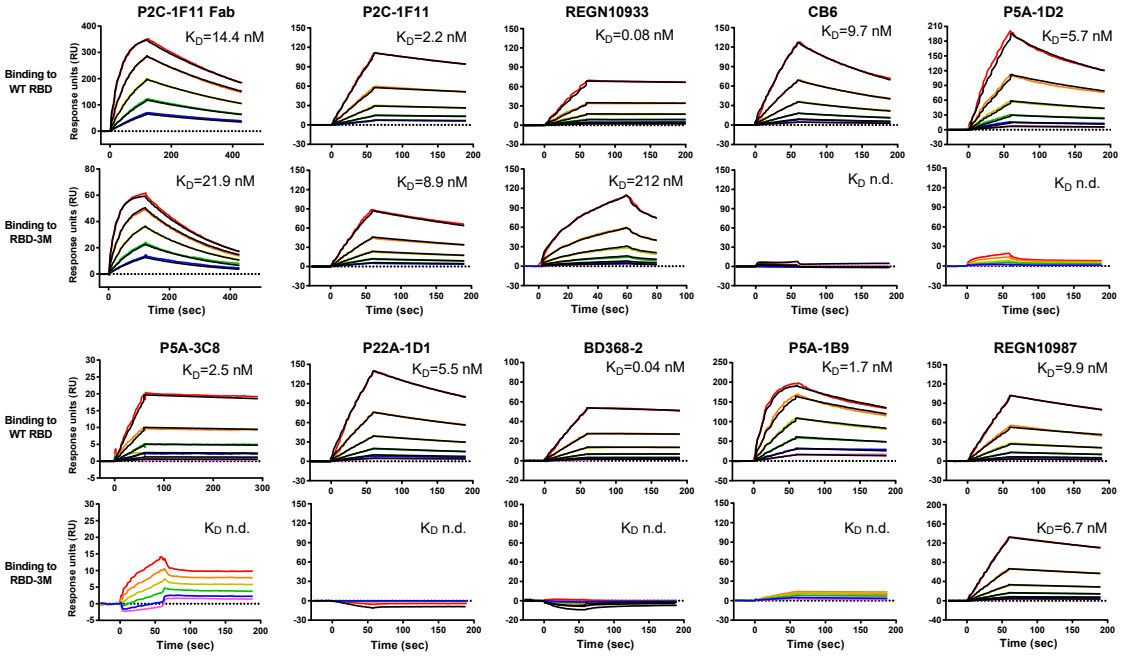

Figure S3.

Binding kinetics of mAb to WT RBD and RBD-3M measured by SPR, related to Figure 2. The Fab and IgG form of mAbs were immobilized on a CM5 sensor and serial concentrations of either wildtype RBD or mutant RBD-3M were flowed through the system. Colored lines indicate the experimentally derived curves. Black lines represent best fitted curves based on the experimental data. The calculated KDs for each mAb are shown against WT RBD and mutant RBD-3M. The names of mAb tested are indicated at the top of each graph.

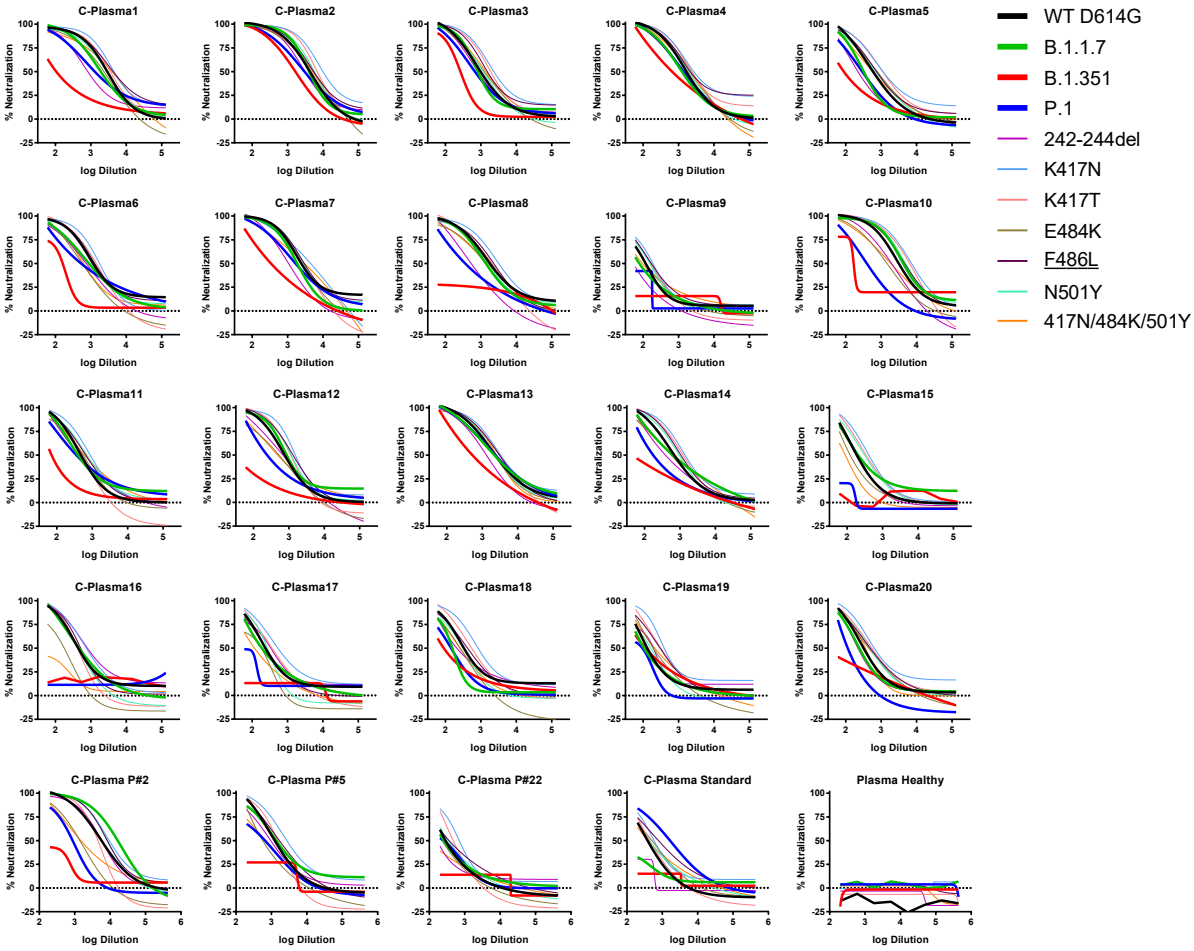

Figure S4.

Neutralization of SARS-CoV-2 variants by each convalescent plasma, related to Figure 3. Pseudoviruses bearing the indicated mutations were tested against serial dilutions of convalescent plasma. Neutralization activity was defined as the percent reduction in luciferase activity relative to no serum control. The actual ID50 and the -fold changes between each mutant and WT D614G pseudovirus were calculated to estimate the resistance levels shown in Figure 3. Results were calculated from three independent experiments.

Table S1. Data collection and refinement statistics (molecular replacement), related to Figure 2.

	RBD-K417N-E484K-N501Y-P2C-1F11 complex
Data collection	
Space group	C2
Cell dimensions	
a, *b*, *c* (Å)	195.844, 85.973, 57.872
a, b, g (°)	90, 99.75, 90
Resolution (Å)	50.00-2.094 (2.15-2.094)[a]
Unique reflections	50710 (3033)
R_{sym} or R_{merge}	0.088(0.384)
I / sI	17.2(3.2)
Completeness (%)	90.92 (54.79)
$CC_{1/2}$ (%)	99.7 (76.2)
Redundancy	5.3 (2.3)
Refinement	
Resolution (Å)	20.98-2.094
No. reflections	50684
R_{work} / R_{free}	16.9/19.7
No. atoms	
Protein	4728
Ligand/ion	14
Water	505
B-factors	
Protein	41.18
Ligand/ion	81.75
Water	46.02
R.m.s. deviations	
Bond lengths (Å)	0.007
Bond angles (°)	0.89
Ramachandran statistics (%)	
Favored	97.19
Allowed	2.64
Disallowed	0.17

[a] One crystal for the data, values in parentheses are for highest-resolution shell.

Table S2. Molecular interaction between P2C-1F11 and mutant RBD-K417N-E484K-N501Y, related to Figure 2.

		P2C-1F11	Length (Å)	Interactions
P2C-1F11/RBD	E/K417/N[N]	H/Y52/CE2[C]	3.84	
		H/Y52/OH[O]	3.87	Hydrogen bond
	E/K417/CG[C]	H/Y52/CE2[C]	3.85	
		H/Y52/CZ[C]	3.97	
		H/Y52/OH[O]	3.32	
	E/K417/CE[C]	H/Y52/OH[O]	3.69	
	E/K417/NZ[N]	H/Y52/OH[O]	3.19	Hydrogen bond
	E/K417/CD[C]	H/Y33/OH[O]	4.02	
	E/K417/CE/[C]	H/Y33/OH[O]	4.03	
P2C-1F11/RBD-3M	E/N417/N[N]	H/Y52/CE2[C]	3.82	
		H/Y52/OH[O]	3.53	Hydrogen bond
	E/Y453/CE1[C]	L/Y33/OH[O]	3.50	
	E/Y453/CZ[C]	L/Y33/OH[O]	3.43	
	E/Y453/OH[O]	L/Y33/CE1[C]	3..58	
		L/Y33/CZ[C]	3..47	
		L/Y33/OH[O]	2.52	
	E/Q493/CG[C]	L/Y33/OH[O]	3.62	
	E/Q493/NE2[N]	L/S32/CB[C]	3.96	
		L/S32/OG/[O]	3.77	
	E/T500/C[C]	L/S28/OG[O]	3.90	
	E/T500/O[O]	L/S28/CB[C]	3.30	
		L/S28/OG[O]	3.01	
	E/Y501/CA[C]	L/S28/OG[O]	3.87	
	E/Y501/CE1[C]	L/V29/O[O]	3.79	
	E/Y501/CZ[C]	L/S30/CA[C]	3.94	
	E/Y501/OH[O]	L/S30/CA[C]	3.82	
		L/S30/CB[C]	3.85	
		L/S30/OG[O]	3.85	

Table S3. Information of the study subjects, related to Figure 3.

Patients	Gender	Age	Severity
C-Plasma1	male	60	severe
C-Plasma2	male	57	severe
C-Plasma3	male	57	severe
C-Plasma4	female	81	severe
C-Plasma5	female	62	mild
C-Plasma6	male	35	mild
C-Plasma7	male	55	mild
C-Plasma8	female	52	mild
C-Plasma9	female	36	mild
C-Plasma10	male	63	mild
C-Plasma11	female	63	severe
C-Plasma12	male	75	mild
C-Plasma13	male	78	severe
C-Plasma14	male	62	mild
C-Plasma15	male	30	mild
C-Plasma16	male	30	mild
C-Plasma17	female	29	mild
C-Plasma18	female	43	mild
C-Plasma19	male	58	mild
C-Plasma20	female	67	severe
C-Plasma P#2	female	65	severe
C-Plasma P#5	female	63	severe
C-Plasma P#22	male	62	mild

Table S4. Primers used in the construction of mutated clones of SARS-CoV-2 S, related to Figure 1.

No.	Primer Name	sequence
1	Mut-1stMS-F	TTGGTACCGAGCTCGGATCCATGTTCCTGCTGACCACCA AGAGAACCATGTTCGTGTTCCTGGTG
2	Mut-S-R	CCACTGTGCTGGATATCTGCAGAATTCTCAGGTGTAGTG CAGCTTCAC
3	nCov-SL18F-F	GTGAGCAGCCAGTGCGTGAATTTCACCACCAGAAC
4	nCov-SL18F-R	GTTCTGGTGGTGAAATTCACGCACTGGCTGCTCAC
5	nCov-SHV69-70del-F	CGTGACCTGGTTCCACGCCATCAGCGGCACCAATGGCAC CAAGAG
6	nCov-SHV69-70del-R	CTCTTGGTGCCATTGGTGCCGCTGATGGCGTGGAACCAG GTCACG
7	nCov-SY144del antisense	CTCTTGTTGTTCTTATGATAAACACCCAGGAAAGGGTCAT
8	nCov-SY144del	ATGACCCTTTCCTGGGTGTTTATCATAAGAACAACAAGAG
9	nCov-SA222V-F	CAGGGCTTCAGCGTCCTGGAGCCTCTG
10	nCov-SA222V-R	CAGAGGCTCCAGGACGCTGAAGCCCTG
11	nCov-S242-244del-F	ACCAGATTCCAGACCCTGCACAGATCATATCTTACAC
12	nCov-S242-244del-R	GTGTAAGATATGATCTGTGCAGGGTCTGGAATCTGGT
13	nCov-SK417N-Fg1251t	CAGGGCAGACCGGCAATATCGCCGAC
14	nCov-SK417N-R	GTCGGCGATATTGCCGGTCTGCCCTG
15	nCov-SK417T-Fa1250c	GGGCAGACCGGCACGATCGCCGACTAC
16	nCov-SK417T-R	GTAGTCGGCGATCGTGCCGGTCTGCCC
17	nCov-SN439K-F	CGTGATCGCGTGGAACTCTAAGAATCTAGATTCGAAA
18	nCov-SN439K-R	TTTCGAATCTAGATTCTTAGAGTTCCACGCGATCACG
19	nCov-SY453F-Fa1358t	GGCAATTACAATTACCTGTTCAGACTGTTCAGAAAGAGC
20	nCov-SY453F-R	GCTCTTTCTGAACAGTCTGAACAGGTAATTGTAATTGCC
21	nCov-SS477N-FG1430A	CTACCAGGCCGGCAACACACCGTGTAATG
22	nCov-SS477N-R	CATTACACGGTGTGTTGCCGGCCTGGTAG
23	nCov-ST478I-F	TACCAGGCCGGCAGCATACCGTGTAATGG
24	nCov-ST478I-R	CCATTACACGGTATGCTGCCGGCCTGGTA
25	nCov-SE484K-Fg1450a	CACCGTGTAATGGCGTGAAGGGCTTCAATTGCTAC
26	nCov-SE484K-R	GTAGCAATTGAAGCCCTTCACGCCATTACACGGTG

Table S4 continued. Primers used in the construction of mutated clones of SARS-CoV-2 S, related to Figure 1.

No.	Primer Name	sequence
27	nCov-SF486L-F	ATGGCGTGGAGGGCTTAAATTGCTACTTCCCTC
28	nCov-SF486L-R	GAGGGAAGTAGCAATTTAAGCCCTCCACGCCAT
29	nCov-SS494P-F	TACTTCCCTCTGCAGCCCTACGGCTTCCAGCC
30	nCov-SS494P-R	GGCTGGAAGCCGTAGGGCTGCAGAGGGAAGTA
31	nCov-SN501Y-Fa1501t	GCTTCCAGCCTACCTATGGCGTG GGCTAC
32	nCov-SN501Y-R	GTAGCCCACGCCATAGGTAGGCTGGAAGC
33	nCov-SA570D-F	CATCTGTGGTGTCGTCGATGTCTCTGCCG
34	nCov-SA570D-R	CGGCAGAGACATCGACGACACCACAGATG
35	nCov-SE583D-F	CCCTCAGACCCTGGATATCCTGGACATCACT
36	nCov-SE583D-R	AGTGATGTCCAGGATATCCAGGGTCTGAGGG
37	H655Y-F	GCCGGCTGCCTGATCGGCGCCGAGTACGTGAATAATAGC TACGAGTGCGACATCCCTA
38	H655Y-R	TAGGGATGTCGCACTCGTAGCTATTATTCACGTACTCGGC GCCGATCAGGCAGCCGGC
39	nCov-SP681H-F	ACCCAGACCAATAGCCATAGAAGAGCCAGAAGC
40	nCov-SP681H-R	GCTTCTGGCTCTTCTATGGCTATTGGTCTGGGT
41	nCov-ST716I-F	TAGCATCGCCATCCCTATCAATTTCACCATCAGCG
42	nCov-ST716I-R	CGCTGATGGTGAAATTGATAGGGATGGCGATGCTA
43	nCov-SS982A-F	GTACTCAACGATATCCTGGCCAGACTGGACAAGGTGGA
44	nCov-SS982A-R	TCCACCTTGTCCAGTCTGGCCAGGATATCGTTGAGTAC
45	nCov-ST1027I-Fc3080t	CCAATCTGGCCGCCATCAAGATGAGCGAGTG
46	nCov-ST1027I-R	CACTCGCTCATCTTGATGGCGGCCAGATTGG
47	nCov-SD1118H-F	GCTCACGAAGGTATTGTGGGTGGTGATGATCTGAG
48	nCov-SD1118H-R	CTCAGATCATCACCACCCACAATACCTTCGTGAGC
49	nCov-SD1163Y-F	CAAGAATCACACCAGCCCTTATGTGGACCTCGGTGATATTT
50	nCov-SD1163Y-R	AAATATCACCGAGGTCCACATAAGGGCTGGTGTGATTCTTG
51	nCov-SV1176F-F	TTCGGGAATCAATGCCAGCTTCGTGAATATCCAGAAGGAAA
52	nCov-SV1176F-R	TTTCCTTCTGGATATTCACGAAGCTGGCATTGATTCCCGAA